Label-free microscale technologies for isolation of heterogeneous circulating tumor cells

Özkayar, G.; Derin, E.; Pesch, G.R.; Martens, J.W.M.; Dijke, P. ten; Boukany, P.E.

ADVANCED NANOBIOMED RESEARCH Open Access
www.advnanobiomedres.com

Label-Free Microscale Technologies for Isolation of Heterogeneous Circulating Tumor Cells

*Gürhan Özkayar, Esma Derin, Georg R. Pesch, John W. M. Martens, Peter ten Dijke, and Pouyan E. Boukany**

The dissemination of primary solid tumor cells to distant organs, termed metastasis, is a major cause of cancer-related deaths. Circulating tumor cells (CTCs), which can exist as individual cells or multicellular clusters, travel through the bloodstream. Their isolation from liquid biopsy samples is increasingly recognized as a valuable tool for diagnosis, prognosis, and treatment guidance for cancer patients. Current isolation methods typically rely on biomarkers like epithelial cell adhesion molecule (EpCAM) and utilize technologies such as magnetic beads or microfluidic chips. However, these methods face limitations due to tumor heterogeneity. Furthermore, tumor cells that transfer into CTCs often undergo epithelial-to-mesenchymal transition, gaining invasive characteristics while losing epithelial markers. As a result, these cells are difficult to detect using EpCAM-based methods. Label-free microscale isolation technologies tackle the limitations of biomarker-based methods by leveraging the distinctive physical properties of CTCs, such as their size, electrical charge, viscoelasticity, and deformability that contrast them from normal blood cells. This review evaluates primary label-free isolation methods, including deterministic lateral displacement, microfiltration, acoustophoresis, and dielectrophoresis, and whether they can offer a deeper insight into tumor heterogeneity and the dynamics of cancer progression and treatment. Additionally, it highlights automated platforms for high-throughput CTC isolation and analysis.

1. Introduction

Solid tumors are characterized by uncontrolled proliferation and/or survival of genomically abnormal cells that can start from any given organ or tissue. Tumor cells can invade adjoining tissue, extravasate into blood or lymph circulation, and subsequently spread and intravasate to distant organs, a process termed metastasis. Metastatic spread of cancers is the leading cause of cancer-related deaths.[1] According to the World Health Organization statistics, in 2018, cancer-related deaths reached 9.6 million worldwide, accounting for every one death in six.[2] Lung, liver, stomach, colorectal, and prostate cancers are the top five most common cancer-related deaths for men worldwide, and breast, lung, colorectal, cervical, and stomach cancers are the top five for women.[2] Besides the tremendous health risk, cancer is expected to cause a substantial economic burden of around 25 trillion US$ between 2020 and 2050.[3,4]

During the metastatic process, circulating tumor cells (CTCs) enter the circulatory and lymphatic systems and spread to distant organs (**Figure 1**A). Isolation and detection of CTCs from the blood may provide insight into the dynamic features of primary tumors and/or metastatic lesions. A liquid biopsy is a body fluid sample (blood, urine, etc.) containing CTCs or tumor cell DNA fragments,[5] which is a powerful source for diagnostics and monitoring disease progression in cancer patients. Regarding the role of liquid biopsies and multiomics analyses in cancer diagnostics, we refer to the review by Visal et al.[6]

The isolation and characterization of CTCs usually require separating cancer cells from regular blood cells in a sample and several particle separation methods have been developed for this purpose. However, several challenges remain for the

G. Özkayar, E. Derin, P. E. Boukany
Department of Chemical Engineering
Delft University of Technology
Delft 2629 HZ, the Netherlands
E-mail: p.e.boukany@tudelft.nl

The ORCID identification number(s) for the author(s) of this article can be found under https://doi.org/10.1002/anbr.202400179.

DOI: 10.1002/anbr.202400179

G. R. Pesch
School of Chemical and Bioprocess Engineering
University College Dublin
Belfield, Dublin 4 D04 V1W8, Ireland

J. W. M. Martens
Department of Medical Oncology
Erasmus University Medical Centre
Rotterdam 3015 GD, the Netherlands

P. ten Dijke
Oncode Institute
Department of Cell Biology
Leiden University Medical Centre
Leiden 2333 ZC, the Netherlands

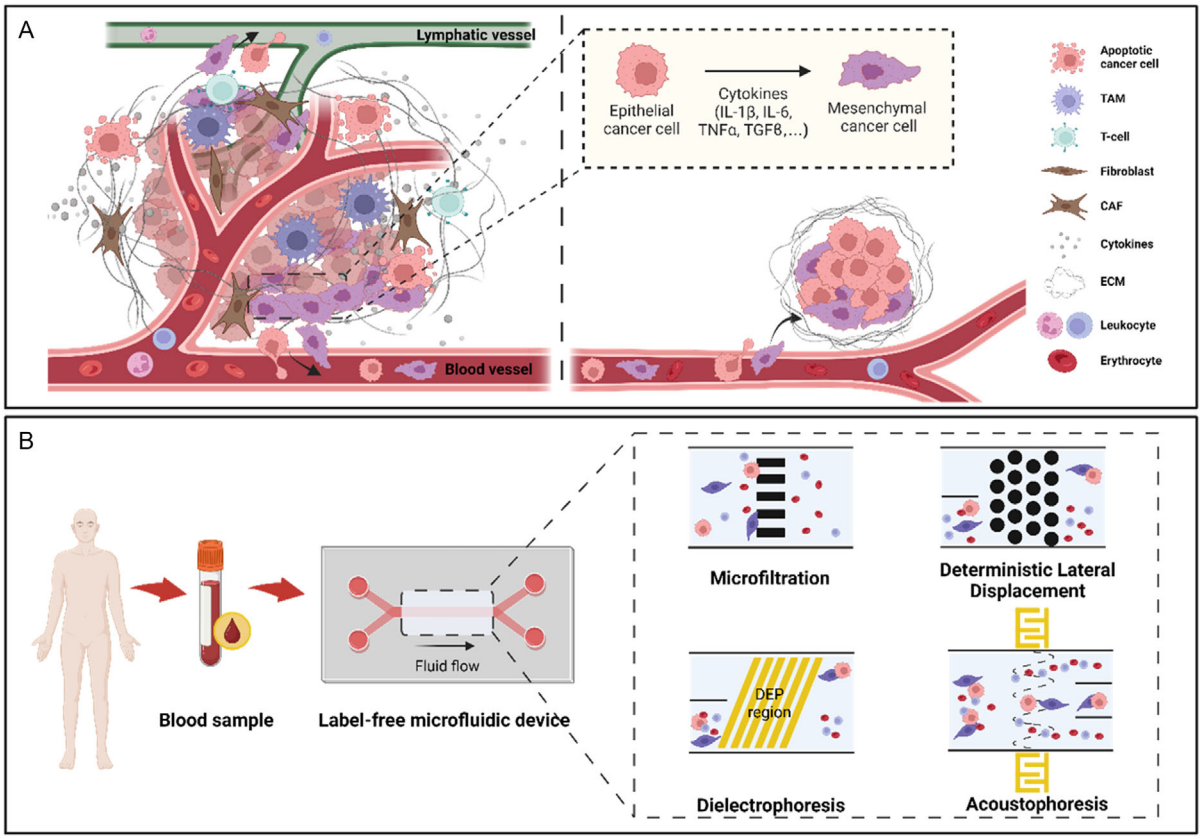

Figure 1. A) Overview of the metastatic process and the role of circulation and CTCs in the spread of cancer; B) Microfluidics-based label-free isolation methods commonly used in liquid biopsy applications. The patient's peripheral blood is collected and processed using specifically designed microfluidic devices based on the biophysical properties of CTCs, against blood cells.

broad application of CTCs in clinical practice, including the low frequency of CTCs in patient blood samples (1–100 cells/mL) and their fragile and heterogeneous nature.[3] The current gold standard and only Federal Drug Administration (FDA)-approved platform for CTC enumeration is the CellSearch system, which uses immunomagnetic enrichment and fluorescent labeling of the captured cells. However, CellSearch can only process 7.5 mL of blood and relies on the presence of the transmembrane glycoprotein epithelial cell adhesion molecule (EpCAM) on the cancer cell. It is thus unable to identify CTCs that do not express EpCAM.[7,8] In addition, the FDA states that CTC enumeration for prognosis can only be used on samples obtained from patients with metastatic breast, prostate, and colorectal cancers.[9,10]

CTC isolation for cancer diagnosis and treatment and the use of liquid biopsy has progressed due to advancements in nanotechnology and microfluidics-based methods.[11] Microfluidic devices are precisely designed and fabricated, often on a size of micrometers (or even nanometers),[12] and they offer reduced sample consumption, quick processing times, simple automation, high throughput, and efficient isolation.[12] These devices can also manipulate small particles such as single cells. Due to precise spatiotemporal control for cell sorting and monitoring, microfluidics has emerged as an appropriate and efficient technological field for CTC separation and isolation.[13,14]

Numerous review articles mainly concentrate on affinity-based isolation of epithelial CTCs using surface markers,[15–18] classifying microfluidic isolation of CTCs in general,[19–22] or only depending on size and deformability.[23] Nevertheless, there is still a need to highlight the recent progress regarding the label-free isolation of heterogeneous CTCs. We do this by first discussing and providing more in-depth data on CTC heterogeneity and highlighting that CTCs generally lack unifying biomarkers. Current commercially available systems to enumerate and isolate CTCs from blood are biomarker-based and, therefore, cannot identify all CTCs.[24] This review demonstrates how label-free isolation techniques (focusing on four common ones displayed in Figure 1B) get beyond the drawbacks of the existing biomarker-based approaches.

In addition, we provide an overview of studies that aim to achieve early diagnosis and (real-time) monitoring of treatment response via downstream analysis, such as enumeration and characterization of various types of CTCs. Next to opportunities, we discuss the challenges of CTC isolation applications using label-free methodologies.

2. Liquid Biopsy—Potentials, Advantages, and Sources

The advantage of liquid biopsy comes from its minimally invasive nature, which enables retrieval of key information regarding

tumor features, heterogeneity, and temporal dynamics. Another advantage is that sample collection and processing are effortless and affordable.[25,26] Although blood is the most common sample in detecting cancer, urine, saliva, nipple aspirate fluids, and synovial and cerebrospinal fluid are also used as liquid biopsy samples.[27,28]

CTCs are cancer cells entering the bloodstream and lymphatic vessels after disseminating from primary and/or metastatic tumor sites. When derived from primary sites, CTCs may lead to metastasis,[29–31] observed in most solid tumors.[29] Besides individual CTCs, CTC clusters or platelets-attached CTCs have also been found in the circulation of patients. Most metastasis studies suggest that CTC clusters are more important for stimulating metastasis than single-individual CTCs.[32–35] Using animal models with tagged mammary tumors, Aceto et al. demonstrated that CTC clusters originate from oligoclonal tumor cell populations rather than through intravascular aggregation events. These CTC clusters had a 23–50-fold higher potential for metastatic spread, while being less common in the circulation than single CTCs.[36] Hu et al. however, by studying clonal dynamics of metastatic progression, revealed that most metastases showed patterns consistent with monoclonal seeding ($n = 151$, 76% of metastases), while polyclonal seeding was less frequent ($n = 48$, 24% of metastases). Given that treatment affects metastasis clonality, they also anticipated that polyclonal seeding of distant metastases would be more prevalent along the metastasis without treatment than in their study.[37]

Through liquid biopsy, selective and efficient isolation and characterization of single CTCs and CTC clusters can be of immense value in diagnosing cancer, determining its prognosis, and studying its evolution.[17] The standard strategy for CTC isolation uses biomarker-mediated platforms (e.g., CellSearch, labeling magnetic beads). However, this approach has the limitation that only CTCs are isolated on which the specific biomarker is expressed at its cell surface, meaning that only specific CTC populations are isolated. The significance of this will be discussed in the following Section 3. Biomarker-independent CTC separation approaches have recently been developed, capable of capturing clinical samples of heterogeneous CTCs by using various approaches such as targeting cell surface electrical charges via functionalized nanoparticles[38] and size-based methods such as microfiltration[39] and inertial focusing.[40,41]

3. Heterogeneity in CTCs

Tumors are known for their heterogeneity and plasticity.[42–48] As cancer cells shed into the bloodstream, they give rise to CTCs with variations in genetic, molecular, and phenotypic features, creating diversity and distinction among individual CTCs.[29,49] Heterogeneity in CTCs refers to the variations in morphology, genetic makeup, molecular markers, and behavior among the CTCs.[50–53]

The existence of heterogeneity in CTCs poses a formidable challenge to the effectiveness of precision medicine and prognosis in cancer.[54,55] Thus, understanding CTC heterogeneity is essential regarding implications for metastasis, treatment response, and developing resistance to therapies.

3.1. Genetic Heterogeneity of CTCs

The genetic makeup of CTCs is comparable to that of the cells in the original and metastatic lesions, according to results from next-generation sequencing and molecular profiling.[29,56–58] The concordance between primary tumors and CTCs is between 62% and 72% for triple-negative breast cancer (TNBC) and 73% and 83% for human epidermal growth factor receptor $(HER2)^+$ tumors;[59] it can reach up to 85% in some cases of breast cancer.[60] The DNA sequence among individual CTCs diverges due to several factors, including the genomic instability of cancer cells,[61] and subclonal evolution within the primary or metastatic tumor.[62,63] Moreover, high-resolution copy number analysis identified that genetic alterations in CTCs showed different metastatic potentials.[6] For instance, individual CTCs from patients with lung cancer were shown to have mutations of the PIK3CA, RB1, and TP53 genes, and CTC sequencing of patients with colorectal cancer revealed mutational variations of the EGFR, KRAS, and PIK3CA genes, indicating that CTCs have dynamic alterations.[64]

Powell et al. highlighted that metastatic sites at various organ locations exhibit unique molecular phenotypes due to qualitative and/or quantitative differences in expression of several genes, likely resulting from intratumoral heterogeneity.[65] They also showed that single-cell phenotyping of CTCs is a feasible way to reveal CTC variability for the success of molecular-guided cancer therapy.

3.2. Phenotypic Heterogeneity of CTCs

Phenotypic heterogeneity covers the variations in the physical and functional characteristics of CTCs, including growth and cell survival rate, presence or absence of cell surface markers, and genetic and epigenetic abnormalities.[45] The distinct differences are also influenced by extrinsic factors (e.g., the tumor microenvironment and therapy provided).[66]

The genetic intricacy of cancer is still being revealed by recently published profiling research, of which the majority is still observational and not described as biomarkers that are linked to clinical outcomes.[67,68] A cancer cell's ability to alter its phenotype without undergoing new genetic changes is known as cancer cellular plasticity and may occur regardless of therapeutic pressure.[69] Research on various kinds of cancer has demonstrated that a neoplastic cell can use developmental processes to adjust to external stimuli.[70,71] Studying the phenotypic heterogeneity in CTCs can help make clinical decisions more effectively. For instance, selecting between the use of an androgen receptor signaling inhibitor and taxane-based chemotherapy in patients with metastatic castration-resistant prostate cancer (mCRPC) may be aided by quantifying the heterogeneity of CTC phenotypes.[72] For instance, McDaniel et al. showed that the $CD45^-/CK^-$ CTC phenotype is common in mCRPC and can offer further prognostic or predictive value besides to the incidence of the generally considered $CD45^-/CK^+$ CTC phenotype.[73]

3.2.1. Role of Epithelial-to-Mesenchymal Transition (EMT) in CTC Heterogeneity

The EMT is an important change that contributes to phenotypic CTC heterogeneity.[52,65,74] EMT is a crucial multistep process

during stem cell biology, wound healing, and embryonic development.[75,76] In this process, epithelial cells acquire the increased motility and invasiveness typical of mesenchymal cells. Cancer cells can also undergo EMT, which increases their ability to migrate and invade. It is a reversible (the latter reverse process is called MET) and dynamic process, also called epithelial-mesenchymal plasticity.[76] Potent stimulators of EMT are hepatocyte growth factor (HGF)/scatter factor and transforming growth factor-β (TGF-β), also causing the loss of transmembrane glycoproteins such as epithelial-specific cadherin (E-cadherin).[77–79]

CTCs from the same tumor can exhibit different expressions of biomarkers, which can change due to the tumor's dynamic nature, such as during EMT. In particular, EMT is associated with the downregulation of epithelial markers (such as EpCAM)[80–82] and the upregulation of mesenchymal markers (such as N-cadherin, vimentin, and caveolin-1),[83–85] making the CTCs more migratory and invasive.

According to a growing body of research, the EMT status of CTCs becomes a reliable candidate for indicating disease progression and survival.[86–92] EMT plays a pivotal role in CTC heterogeneity by creating hybrid epithelial–mesenchymal phenotypes (E/M-CTCs), enabling adaption to new microenvironments during metastasis.[74] In prostate, breast, and lung cancers, the data from human samples highlight the presence of E/M-CTCs in heterogeneous CTC populations.[93,94] By quantitatively comparing the predicted prognostic capacity of epithelial phenotypes (E-CTCs), mesenchymal phenotypes (M-CTCs), and hybrid epithelial–mesenchymal phenotypes, Sun et al. suggested E/M-CTCs show predictive value for metastasis and survival in pancreatic ductal adenocarcinoma.[86] Jolly et al. suggested that the E/M-CTC phenotype fosters the collective migration of CTC clusters.[95] Among breast cancer subtypes, the ones with a poor clinical outcome, that is, TNBC and basal-like breast cancer, are the ones enriched for E/M-CTCs, indicating that E/M-CTCs are linked to aggressive behavior.[96,97] Disease progression and therapy resistance increase when M-CTCs outnumber E-CTCs in CTC counts.[96] On the other hand, E/M-CTCs likely correlated with worse prognosis by acquiring the ability to self-renew, and they present higher resistance to chemotherapy compared to E-CTCs and M-CTCs.[34,95]

3.3. Morphological Heterogeneity of CTCs

Individual CTCs are observed in similar shapes with white blood cells (WBCs),[98] from round to oval,[99] and usually have a wide range of diameters larger than 5 μm.[100] Mendelaar et al. showed that four different cancer types, including breast, prostate, colorectal, and bladder cancers, have varying median E-CTC sizes. The study was done using CellSearch and contained a total of 71 612 events. Measured median sizes are 12.4 μm for breast cancer, 10.3 μm for prostate cancer, 7.5 μm for colorectal cancer, and 8.6 μm for bladder cancer.[101]

Patients may also display CTC clusters in various malignant neoplasms, which are microemboli (spheroids) made up of 2–50 cells.[29] Thirty to 40% of patients with melanoma or metastatic breast or prostate cancer were reported to have CTC clusters.[102] The narrow detection window and lack of suitable detection methods for CTC clusters may mean their occurrence and quantity are underestimated. In addition, CTC clusters originating from primary breast and prostate cancers might contribute to those cancers showing poor prognosis.[36] Wendel et al. found that the nuclear diameters of CTCs in clusters across stages I–VI are comparable and that 32–47% of CTCs in nonsmall cell lung cancer (NSCLC) form and migrate in clusters.[103] CD44, intercellular adhesion molecule 1, and epigenetic reprogramming are among the stimuli that provide CTC clusters with increased self-renewal capacity, as well as plasticity. Both homo- and heterotypic CTC clusters were observed;[104] heterotypic clusters were composed of immune cells, cancer-associated fibroblasts, and platelets in addition to CTCs.[105–107]

4. Isolation, Sorting, and Enumeration Technologies for CTCs

The separation and counting of CTCs opens the possibility to improve cancer diagnosis, early detection, prognostication, and monitoring of treatment outcomes. However, this remains challenging. Microfluidic methods for isolating and enumerating CTCs from liquid biopsies are especially promising as they allow to efficiently and continuously isolate CTCs from hematological cells.[108,109]

Various research groups and companies have recently proposed several microfluidic technologies to advance CTC isolation. While these technologies hold significant promise for cancer healthcare, most CTC methods are still primarily used for research purposes. Only a limited number of methods have been approved for clinical use, mainly due to challenges posed by CTC heterogeneity, their rarity in blood, and the lack of comprehensive clinical validation.[110] The consequential challenge of CTC isolation is their rarity among blood cells; a 10 mL peripheral blood sample from a metastatic cancer patient can potentially contain 1–10^4 single CTCs[99,111,112] and/or roughly 0–5 CTC clusters.[113,114] However, the same sample includes a high number of blood cells, including leukocytes (4.0–11.0 × 10^7), erythrocytes (4.5–5.6 × 10^{10}), and platelets (1.5–4.0 × 10^9),[115] which makes full recovery of pure CTCs from whole blood quite demanding. Another challenge is CTC heterogeneity. Label-based isolation techniques (Section 4.1) have enabled successful isolation of CTCs based on the expression of certain membrane glycoproteins, such as EpCAM. However, as outlined in Section 3, CTCs are highly heterogeneous, and not all CTCs express the marker used. Thus, these latter CTCs potentially escape by using a marker-based isolation technique. Furthermore, CTCs may not be uniform in size, and not all CTCs are significantly larger than regular blood cells, making size-based isolation challenging.

CTC isolation strategies can be distinguished into two categories: label-based isolation, which relies on an affinity-based interaction and label-free isolation, which utilizes the physical properties of cells.[116] Due to the challenges of capturing all types of CTCs due to phenotypic heterogeneity, this review only provides a brief overview of label-based isolation techniques (Section 4.1) and describes label-free isolation techniques in more detail (Section 4.2).

4.1. Label-Based Isolation Techniques

Label-based CTC isolation techniques target CTCs using antibodies, offering advantages like high specificity, sensitivity, and automation.[117–119] These techniques can be divided into positive and negative isolation strategies. Positive isolation strategies target cancer-specific markers on the cell membrane, such as epithelial markers (e.g., EpCAM,[120] E-cadherin,[121] and cytokeratins (CKs)[122]), mesenchymal markers (vimentin[123] and N-cadherin[124]), or cancer type-specific markers (i.e., HER2 for breast cancer,[125] prostate-specific membrane antigen for prostate cancer,[126] CD147 for kidney cancer,[127] and carcinoembryonic antigen for colorectal cancer).[117,128] EpCAM or CK expression levels vary among CTCs, with some showing the total downregulation of both proteins (e.g., during EMT), which limits the efficiency of detection and isolation based on those markers.[55] In contrast, negative selection methods target $CD45^+$ cells for subsequent removal.[129] The fundamental idea behind the negative selection technique is to eliminate all cells besides CTCs, mainly the depletion of leukocytes by targeting CD45 and CD66B molecules.[116,130–132] While this technique effectively depletes non-CTCs, it often results in lower recovery of CTCs. Therefore, this isolation technique is usually combined with other label-free isolation techniques.[133,134]

4.2. Label-Free Isolation Techniques

Label-free isolation techniques are based on biophysical characteristics of CTCs which relate to differences in size, density, deformability, and electrical properties, allowing for the distinction of CTCs from other cell types without labeling.[55,135] These techniques offer minimal manipulation, fast processing times, and less complexity[136,137] and may enable a better potential for clinical feasibility and validity by enhancing the performance of CTC isolation.[135]

Label-free isolation techniques can be either active or passive. The active methods use various external forces, that is, ultrasound, electrical, or magnetic fields. Examples are acoustophoresis[138] and dielectrophoresis (DEP).[139] The passive methods (relying on the structure of fluidic geometry) often utilize pillars and objects within microchannels to separate and isolate CTCs without external force fields. Examples include adhesion-based methods,[140] pinched-flow fractionation,[141] inertial forces,[41,142,143] and biomimetic separation.[144]

Four of these label-free techniques have become widely recognized: deterministic lateral displacement (DLD)-based isolation, filtration-based isolation, acoustophoresis-based isolation, and DEP-based isolation. This review extensively examines these four primary label-free isolation methods.[135] Each technique offers distinct advantages and challenges for isolating CTCs while accounting for their heterogeneous nature. The performance of these techniques, as well as their advantages and disadvantages, is discussed and summarized in **Table 1**.

4.2.1. DLD-Based Isolation

DLD is a high-throughput and noninvasive method for CTC isolation. Its key strength lies in its ability to separate CTCs from blood samples based on size[145,146] and deformability.[144,147] This makes DLD especially effective when there is a clear size difference between the CTCs and other cells in the sample. It was first used in 2004 for biological (e.g., eukaryotic cells, spores, bacteria, viruses, DNA, vesicles) and nonbiological (e.g., droplets) particle separation in continuous flow. This separation method relies on controlling the motion trajectory of the particles by placing a post inside the microchannel.[144,148]

Loutherback et al. studied the shapes of posts and presented that triangular posts, compared to the circular ones, enhanced the performance by lowering the hydrostatic pressure needs and expanding the range of displacement characteristics.[149] In addition to geometry (e.g., pillar shape, the gap between pillars, microchannel depth, length, and width), material properties (e.g., surface treatment, permeability, and deformation), flow characteristics (e.g., velocity, pressure, and hydraulic resistance), and sample type (particle size and deformation, concentration, heterogeneity, interactions and buffer) are key parameters for the design, fabrication, and operation of DLD-based isolation devices.[148]

In DLD microfluidics, pillars are fabricated with row shift fraction, which generates fluid bifurcation and a unique number of streamlines between the gaps. The number of streamlines between each pillar corresponds to the periodicity of the DLD array because the total fluid flow on each gap can be divided by the periodicity (N). Fluidic forces and pillar obstacle effects are the two main parameters that affect particle flow. When two different particles are placed in a pillar gap in the DLD array, a particle that is smaller than the first streamline width will follow the first streamline and move in a zigzag pattern. The second particle, bigger than the first streamline width, will bump against the pillar and move laterally to the next streamline (**Figure 2**A). The DLD critical diameter (D_c), which can be easily adjusted by arranging lateral and downstream pillar gaps (D_x, D_y, and G), the row shift fraction (ε), and the pillar diameter (D_0), determines the zigzag and displacement mode of the particle (Figure 2A).[150] Holmes et al. defined the DLD mechanism as particles smaller than the critical diameter moving in the flow direction and particles larger than the critical diameter moving according to the pillar arrangement.[151] Zhang et al. simulated red blood cell (RBC) trajectories with diverse pillar shapes, including circular-, diamond-, and square-post arrays. In contrast to rigid spherical objects, biological components are deformable, not perfectly spherical, which influences their trajectories in DLD devices.[152]

Au et al. presented a continuous flow microfluidic device for isolating intact CTC clusters from whole blood using a DLD mechanism.[153] The first stage of the mechanism consists of a regular DLD array having cylindrical pillars with a 90 μm channel height to separate large clusters based on size, and the second stage covers asymmetric pillars with a 30 μm channel height to separate small clusters (Figure 2B). They claimed that cultured breast cancer CTC clusters containing 2–100+ cells (having size heterogeneity) can be recovered with 99% efficiency and 87% cell viability from RBCs. Liu et al. reported on a combined filter-DLD strategy for high-throughput and label-free CTC isolation in one step from advanced nonsmall cell lung cancer (NSCLC) patients.[154] Differently from standard DLD devices, they used a hydrodynamic cell sorting design by adding a filtering mechanism into a DLD structure that enabled high-throughput and

Table 1. Assessment of different microfluidic methods for CTCs isolation considering cancer types, sample sources, results, and limitations.

Isolation method	Working scheme	Cell types	Sample sources	Obtained results	Limitation	Reference [s]
DLD	Two-stage continuous microfluidic chip	Breast cancer cells isolated from patients' blood	Spiked in PBS Spiked in blood	99% recovery High cell viability (87%)	Low throughput (0.5 mL h^{-1})	[153]
	Filter DLD microfluidic chip	A549[a] K562[b]	Spiked in diluted blood	>96% recovery 100 cells/mL High cell purity (WBC removal rate 99%) High cell viability (>98%) High throughput (1 mL min^{-1})	Validation with diluted blood samples	[154]
	Circular and triangular DLD arrays	MCF-7[c] MDA-MB-231[d]	Spiked in diluted blood	99% recovery for MCF-7 80% recovery for MDA-MB-231 ≈104 cells/ml High throughput (2 mL min^{-1}) High cell viability	Validation with diluted blood samples (10 times) Limited isolation with highly viscous samples	[146]
	Inertial microfluidic integrated DLD chip	MCF-7	Spiked in diluted blood sample	≈92% recovery ≈104 counts mL^{-1} High purity (94%) Relatively high throughput (400 µL min^{-1})	No isolated tumor cell with low concentration (500 counts mL^{-1}) Only one cell type (Not heterogeneous)	[158]
	Triangle array	MCF10A[e] MDA-MB-231	Spiked in buffer Spiked in diluted blood	85% recovery High throughput (10 mL min^{-1})	Preprocessing of blood samples from patient Validation with diluted blood samples	[145]
	Diagonal physical barrier	A431[f] SK-BR-3[g]	Spiked in anti-coagulated whole blood	> 95% recovery High throughput (5 mL min^{-1})	–	[216]
Filtration	Micropore-arrayed filtration-membrane	A549	Spiked cell in PBS Unprocessed BALF Whole blood	86.2 ± 4.8% recovery ≈100 cells mL^{-1} High recovery rate with lower cell concentration (≤ 3 cells 10 mL^{-1} - 83.3%) High throughput Validation with blood samples from lung cancer patients	Only one cell type (Not heterogeneous)	[217]
	Conical-shaped holes	MCF-7 HT-29[h] U87[i]	Spiked in PBS diluted healthy human blood	≈95% recovery ≈95% cell viability after isolation	Low purity Membrane clogging Distinct size of CTC Difficult to detach CTC from the filter	[55,164]
	Prefilters and cell isolation filters	SW480[j]	Spiked in whole blood	70% recovery 100 cells/3.75 mL High throughput	Blockade risk on the filters with high viscous samples (e.g., whole blood)	[168]
	Tapered slit filter	HT-29 MCF 7 SW620[k] MDA-MB-231	Spiked cells in PBS Spiked cells in diluted blood	83–100% recovery High throughput (25 mL h^{-1}) High viability (87–94%)	Elevated risk of clogging	[218]
	Filtration microchannels	A549 SK-MES-1[l] H446[m]	Spiked cells in PBS Spiked cells in whole blood	96% recovery for A549 95% recovery for SK-MES-1 92% recovery for H446 High efficiency	Preprocessing of blood samples from patient Low throughput (0.4 mL h^{-1})	[55,219]
	Ultra-thin silicon nitride membrane	A549 MCF-7	Spiked cells in PBS Spiked cells in whole blood	82 ± 1% recovery for A549 86 ± 3% recovery for MCF-7 High throughput (1 mL min^{-1})	Elevated risk of clogging	[220]

Table 1. Continued.

Isolation method	Working scheme	Cell types	Sample sources	Obtained results	Limitation	Reference [s]
	Meshed microwells	MDA-MB-231 MCF-7, LNCAP[n)], HeyA8[o)]	Spiked in whole blood	≈90% recovery High throughput (>25 mL h^{-1}) High viability (≈95.8%)	Complicated and multistep fabrication	[114]
	PDMS membrane filter	A549 SK-MES-1 H446	Spiked in PBS Peripheral blood	90% recovery High throughput (10 mL h^{-1}) Easy and cost-efficient fabrication of membrane	Low resolution with PDMS-based membrane	[221]
Acoustophoresis	taSSAW	MCF-7 HeLa[p)]	Spiked cells Peripheral blood	83% recovery ≈100 cells mL^{-1} Validation with cancer patient samples A relatively higher volume (≈20 times to similar principle)	Preprocessing of blood samples from patient	[222]
	Array of acoustic microstreaming traps	MCF-7 MDA-MB 231	Spiked cells in PBS Spiked cells in diluted blood	95 ± 5% recovery in PBS 66 ± 4% recovery in whole blood sample Ability to isolate both epithelial and mesenchymal cell lines High cell viability (96%) after 10 min ultrasound-treatment	Low throughput (12 µL min^{-1}, 1200 µL for 10 min)	[178]
	Thin-ultrasonic-separator-chip; plate acoustic waves	Panc-1[q)]	Spiked cells in PBS Spiked cells in RBC-lysed blood samples	84% ± 8% recovery High viability (85%) Relatively high throughput (80 µL min^{-1})	Stability of the pressure node The requirement for chip symmetry	[223]
	Acoustic impedance contrast by lead zirconate titanate transducer	HeLa MDA-MB-231	Peripheral blood mononuclear cells	>86% recovery	Low throughput (30–20 µl min^{-1})	[224]
	Piezoceramic transducer-based microfluidic chip	DU145[r)] PC3[s)] LNCaP	Spiked cells in erythrocyte-lysed blood sample	93.6–97.9% recovery High purity (97.4–98.4%)	Low throughput (100 µL) Not validated with the clinical sample	[225]
DEP	Dielectrophoretic field-flow fractionation (ApoStream)	SKOV3[t)] MDA-MB-231	Spiked into PBMC	50–75% recovery Clinically relevant throughputs Very low number of cells spiked into PBMC	–	[193]
	Clinical sample studies using ApoStream	ASPS[u)][196] Adenocarcinoma[197] Breast Cancer[197,198] Ovarian cancer[197] Squamous Lung Cancer[197]	Blood samples from patients	ApoStream is capable of recovering CTC from patient blood samples with different tumors. Study on clinical samples. Heterogeneity in CTC recovered from breast cancer patients is addressed[198]	–	[196–198]
	cDEP	MCF10A MCF-7 MDA-MB-231	Cells separated from each other	Cells are not in contact with electrodes, avoids electrochemical effects Separation of three different human breast cancer cell lines to mimic cancer progression	Feasibility study	[143]
	cDEP	MOSE-L[v)] MOSE-LTICv[w)]	Cells separated from each other	Separation of cancer cell subpopulations and isolation of highly aggressive cancer subpopulation	Feasibility study	[200]

Table 1. Continued.

Isolation method	Working scheme	Cell types	Sample sources	Obtained results	Limitation	Reference [s]
	iDEP	MCF-7 MDA-MB-231	Cell lines separated from each other	Separation of two human cell lines	Feasibility study	[190]
	DEP-based lateral displacement	PC14PE6/AS2-GFP[x)]	Cells spiked into WBC and RBC	50–90% recovery depending on flow rate High flow rates High recovery efficiencies	Low isolation purity Low total cell density	[202]
	DEP at a wireless electrode array	MDA-MB-231	Spiked cells	Wireless electrode array usage	Single cell capture Possibility to scale to clinically relevant throughputs Jurkat E6-1 T cells as model for WBCs	[201]
	Optically induced DEP	PC-3 OECM-1[y)]	Spiked in sucrose solution	76–83% recovery for PC-3 cells 61–68% recovery for OECM-1 cells High viability 94% for PC-3% and 95% for OECM-1 cells	Low throughput (6 μL h^{-1} and sample volume: 1 μL) Relatively low purity (PC-3 cells: 74–82%, OECM-1 cells: 64–66%)	[226]

[a)]A549: lung cancer. [b)]K562: myelogenous leukemia. [c)]MCF-7: breast cancer. [d)]MDA-MB-231: breast cancer. [e)]MCF10A: breast cancer. [f)]A431: lung cancer. [g)]SK-BR-3: breast cancer. [h)]HT-29: colon cancer. [i)]U87: glioblastoma (brain cancer). [j)]SW480: colorectal cancer. [k)]SW620: colorectal cancer. [l)]SK-MES-1: lung cancer. [m)]H446: lung cancer. [n)]LNCaP: prostate cancer. [o)]HeyA8: ovarian cancer. [p)]HeLa: cervical cancer. [q)]Panc-1: pancreatic cancer. [r)]DU145: prostate cancer. [s)]PC-3: prostate cancer. [t)]SKOV3: ovarian cancer. [u)]ASPS: alveolar soft part sarcoma. [v)]MOSE-L: murine ovarian cancer-slow developing. [w)]MOSE-LTICv: murine ovarian cancer-fast developing. [x)]PC14PE6/AS2-GFP: lung adenocarcinoma. [y)]OECM-1: oral squamous cancer.

clog-free isolation. The filtering mechanism altered the fluid field around the DLD microposts, allowing more precise manipulation of cell motion. The separation efficiency was >96% with a near complete WBC removal rate. In addition, high cell viability (>98%) was observed at a 1 mL min^{-1} flow rate.

In another DLD-based isolation device, triangle posts were used inside the channel under continuous flow by using breast cell lines MCF10A and MDA-MB-231 and prostate cancer cell line PC3.[145] The recovery rate was 85% for fluorescently labeled MDA-MB-231 breast cancer cells which were spiked into diluted whole blood (10:1). They followed a trajectory in an array when a 500 μL min^{-1} flow rate was applied (Figure 2C).

DLD-based CTC isolation is often integrated with other approaches for CTC retrieval, such as magnetic nanoparticles,[155] DEP,[156] impedance cytometry,[157] and inertial microfluidics.[158] Beech et al. developed a DLD-based microfluidic system with electrically coupled metal-coated posts to enhance separations drastically reducing the critical size for separation and improved the dynamic range of the DLD system.[156] This platform enabled a reduction in the critical particle size. When particle size is close to critical diameter, a slight external force is sufficient to move particles to another trajectory. The metal coating on the pillars allows voltage to be applied and produces electric field gradients between adjacent posts, which causes polarizable particles to be subject to a DEP force. The volume and polarizability of the particle determine the generated DEP force which is strong enough to drive particles from one streamline into another. This allows for tuning a device's critical size, typically defined by geometry. This platform can also find applications in CTC isolation since both methods are widely used.

In addition, Xiang et al. integrated inertial microfluidics and DLD principles in a two-stage i-DLD sorter to separate MCF7 cell line cells from WBCs precisely and continuously in diluted whole blood.[158] A spiral inertial microfluidic sorter enabled the removal of the main background (blood cells) in a high-throughput manner. The DLD section comprises triangular posts that efficiently remove the remaining blood cells to acquire higher purity for CTC retrieval. The stained MCF-7 cell line cells were collected at outlet III (Figure 2D).

The advantages of DLD are that, depending on the application, the technique does not require any pretreatment or dilution procedures. For example, Campos-Gonzales et al. showed that DLD can separate platelets directly from whole blood.[159] The limitations of DLD include the potential for reduced separation efficiency when dealing with smaller or highly deformable CTCs that resemble normal blood cells.[160] Additionally, traditional DLD may not be sufficient for distinguishing CTCs from other circulating cells with similar sizes, since the geometry cannot be easily modified,[161] making a combined approach necessary in which DLD is combined with another isolation technique (as described in this section).

4.2.2. Filtration-Based Isolation

Filtration is a simple and cost-effective method for isolating CTCs by exploiting differences in cell size. Advancements in filtration technology in the 1960s led to the development of polymer-based membranes, with controlled pore sizes, thanks to the introduction of track-etching processes.[162] Controlling pore size enables the exact separation of particles based on size

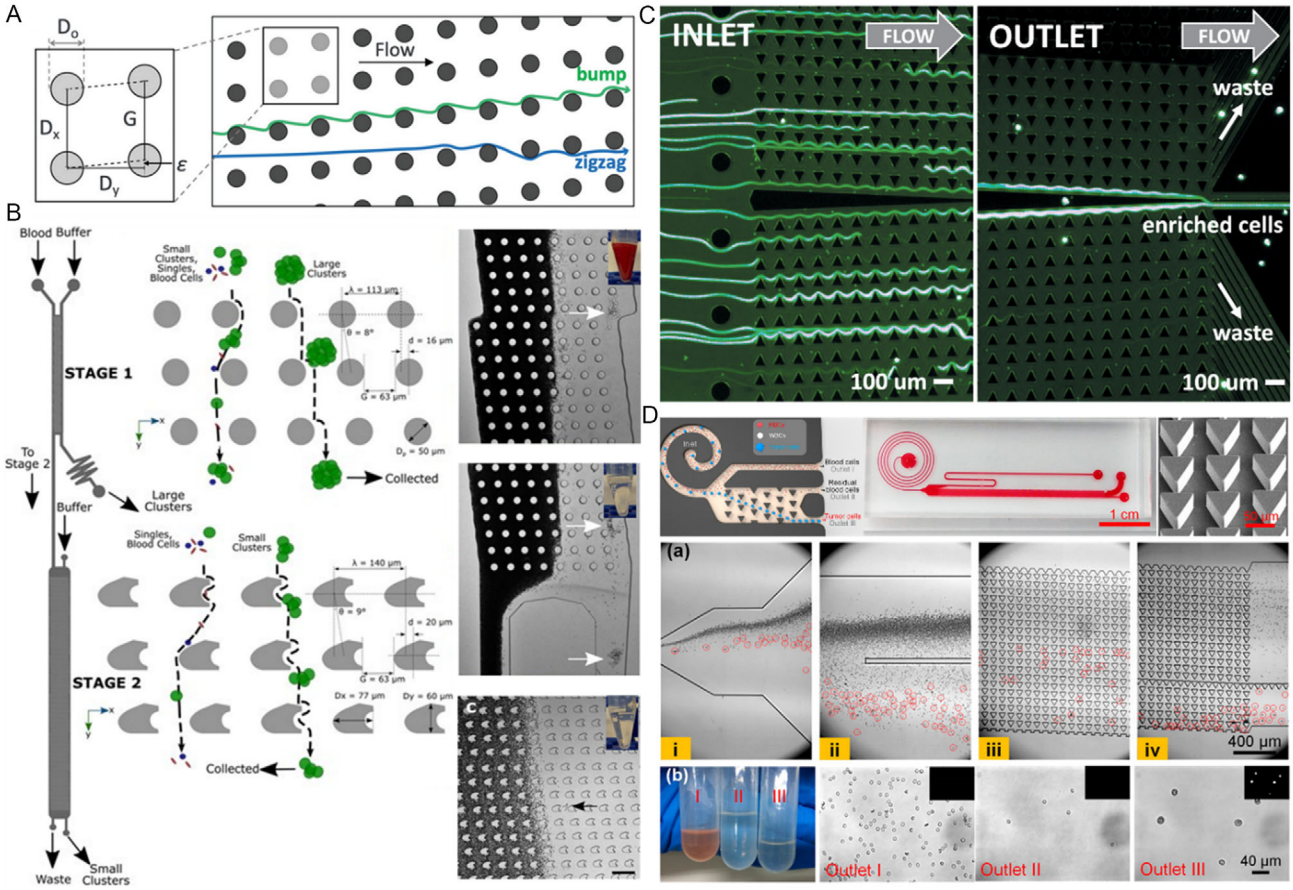

Figure 2. The method of DLD-based isolation and studies. A) DLD diagram showing important geometrical design elements that affect particle paths. The zigzag mode, in which net particle trajectories are unaffected by the array and maintain their average transverse position along the flow direction, and bump mode, in which the pillar array displaces; particles are the two canonical translocation modes for DLD shown in the array schematic. The DLD array was designed so that particles with a diameter greater than the critical diameter enter a bump mode and are pushed to the edge of the array. This latter process is essential for particle concentration and isolation. Reproduced with permission.[215] Copyright 2021, John Wiley and Sons. B) Stage 1 and stage 2 device inlet, outlets, and fluidic paths. The cylindrical micropillars in stage 1 deflect large clusters from other blood cells using DLD. An array of asymmetric pillars in stage 2 deflects small clusters. Reproduced under terms of the CC-BY license.[153] Copyright 2017, Au et al. published by Springer Nature. C) Enrichment of CTCs in a DLD array. MDA-MB-231 cells are evenly distributed at the inlet, and then they are manipulated towards the central wall by the triangular DLD array. Reproduced under terms of CC-BY license.[145] Copyright 2012, Loutherback et al. published by AIP Publishing. D) Workflow of the two-stage i-DLD device combines the spiral inertial microfluidic sorter with the DLD sorter to separate tumor cells from background blood cells. Photograph of the final device fabricated in polydimethylsiloxane (PDMS) using soft lithography, microfluidic device (filled with red ink), and scanning electron microscope (SEM) image of the fabricated triangular posts and isolated CTCs (in red circles). Reproduced with permission.[158] Copyright 2019, American Chemical Society.

differences. Microfluidics enabled the implementation of various filtration-based platforms to isolate different particles, including bioparticles such as cells.

Kang et al. used tapered gaps in slits to create a filter.[163] Unlike traditional straight-hole filters, these tapered gaps feature a wider entrance that gradually narrows, reducing cell stress. The performance of this platform was validated by spiking H358 cancer cell lines into phosphate-buffered saline (PBS) and diluted blood (1:4) at a concentration of 10^5 cells ml^{-1}, achieving efficiencies of 90% and 82%, respectively. After 5 days, cell viability remained at 72%, indicating potential for downstream analyses. A similar method was introduced by Tang et al. who developed a microfilter with conical-shaped holes with crossflow components (**Figure 3**A). Cell capture efficiency of the filters was tested by using HT-29, MCF7, and U87 cancer cell lines separately spiked into PBS with concentrations of 100 cells ml^{-1}. Clinical validation was done using 15 cancer patients and 6 healthy donor blood samples. CTCs were captured from 66% of the patients, and no CTC capture was observed on healthy donor samples.[164] Isolating single cells using only filtration-based technologies is challenging, especially in whole blood as CTCs and some leukocyte types (like neutrophils and monocytes) are similar in size, making separation difficult. As a result, most size-dependent platforms target CTC clusters. Sarioglu et al. introduced a cluster chip featuring an array of triangular pillars with bifurcating traps to create confined regions to isolate CTC clusters. MDA-MB-231 cancer cell clusters were added to whole blood samples and capture efficiencies were calculated as 99% for large clusters (>4 cells), 70% for 3-cell clusters, and 41% for 2-cell clusters.[102]

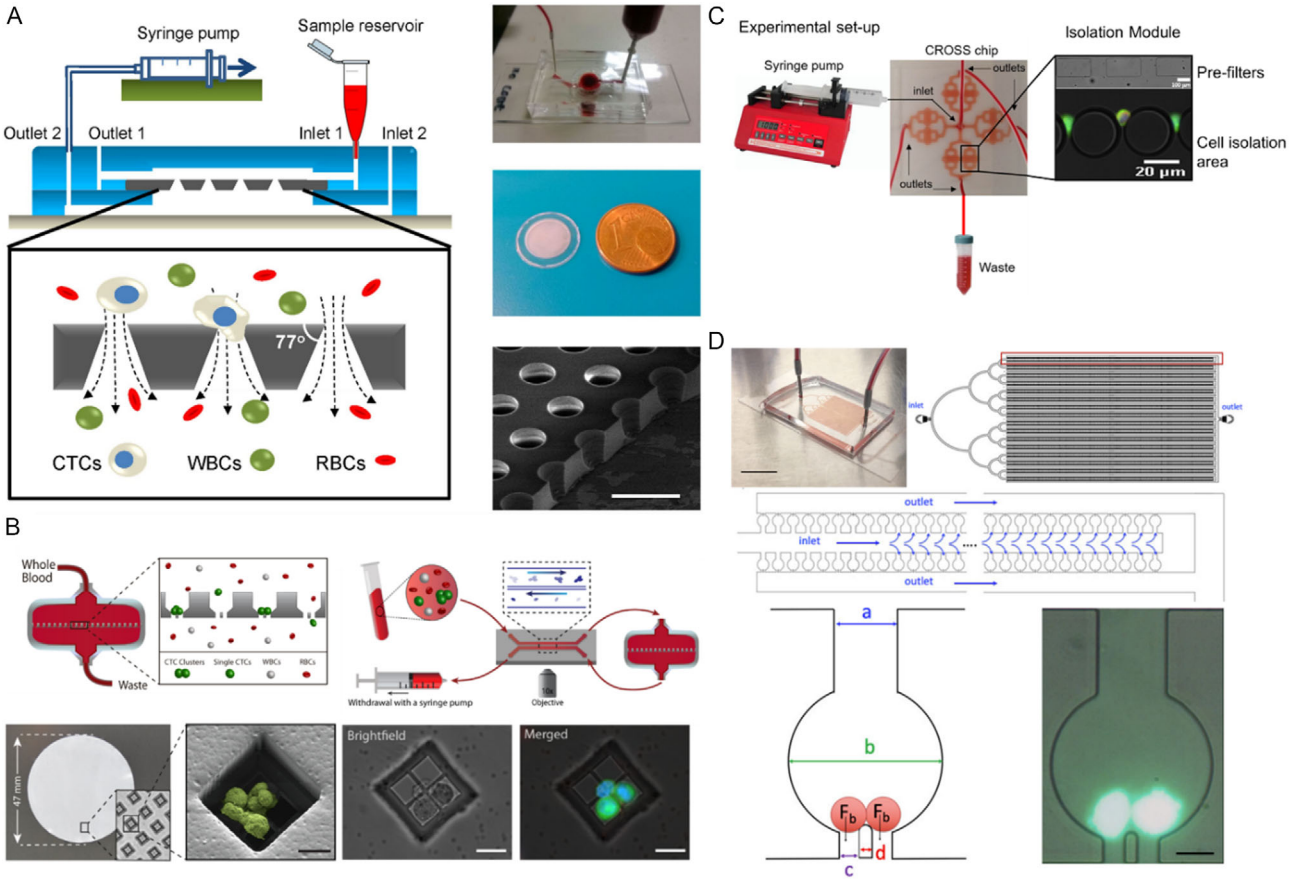

Figure 3. The working principle of filtration-based isolation. A) Illustration of integrated conical-hole filter to capture CTCs. Picture of microfluidics using a test blood sample in operation and comparison with one euro cent coin and SEM image of conical holes array (scale bar: 40 µm). Reproduced with permission.[164] Copyright 2014, Springer Nature. B) Representation of Cluster–Wells working principle and experimental setup. The Cluster–Wells catch CTC clusters from blood samples of cancer patients, regardless of the type of malignancy and its molecular component, whereas single cells pass through unhindered. SEM image of blood-spiked LNCaP prostate cancer cell cluster as captured by one of the wells on the device (Scale bar: 20 µm). Reproduced under the terms of the CC-BY license.[114] Copyright 2022, Boya et al. published by Springer Nature. C) Experimental setup for CTC isolation using the CROSS chip. Reproduced under the terms of the CC-BY license.[168] Copyright 2019, Ribeiro-Samy et al. published by Springer Nature. D) The image of the microfluidic isolation of CTC clusters device (scale bar: 10 mm). The device was designed using computer-aided design software (AutoCAD). It comprises three sections: a left-side input section for spreading flow, a middle-section capture portion for capturing tumor cell clusters while blood flows through it, and a right-side outflow section. F_b acts as a balancing force when a binary cluster comes into contact with a pillar that splits the flow in two. Captured fluorescent stained CTC clusters were imaged in the trap chamber (scale bar: 50 µm). Reproduced with permission.[170] Copyright 2019, AIP Publishing.

The corners of square filters may impose considerable tension on passing cells, as demonstrated by Kim et al.[165] who presented a reversibly deformable membrane barrier for CTC isolation with a 94% retrieval efficiency, even at very low cell concentrations (≈10 cells/0.1 mL). For capture efficiency tests, four cell lines were used, two of them are lung cancer cell lines (H358 and H460), and the other two are colorectal adenocarcinoma cell lines (LoVo and SW620). Blood samples from two lung cancer patients and five colorectal cancer patients were also collected, and the number of detected CTCs was up to 158.

Liu et al. proposed an innovative release strategy using a magnesium (Mg)-embedded cell filter that can be etched in PBS or Dulbecco's modified Eagle medium. MDA-MB-231 breast cancer cell lines were used to check the filter efficiency. A total of 29 cells were spiked into 0.4 mL PBS, and about 90% capturing efficiency was obtained.[166]

Boya et al. combined the efficiency and practicality of membrane filtration with the deterministic screening capabilities of microfluidic chips in a system called Cluster–Wells for CTC isolation from whole blood samples.[114] The Cluster–Wells contain ≈100 000 microwells with 15 µm openings, which physically capture CTC clusters present in unprocessed whole blood, isolating almost all clusters at a flow rate exceeding 25 mL h^{-1} while enabling the retrieval of viable clusters (Figure 3B). The study reported isolation of CTC clusters containing 2–100 + CTCs from lung and colorectal cancer patients. Similar to the Cluster–Well mechanism, microcavity structures were utilized by Hosokawa et al. for CTC isolation based on cell size. CTC detection efficiencies for the microcavity system were 77% for NSCLC patient samples and 95% for SCLC patient samples, compared to CellSearch's detection efficiency of 32% for NSCLC patient samples and 57% for SCLC patient samples.[167]

One recent study implemented a two-stage filtration method using a cross-shaped design.[168] Each chip consists of four sections containing prefilters (120 μm gaps) and cell isolation filters, which feature a single row of 25 μm anisotropic micropillars spaced 5 μm apart (Figure 3C). Based on size and deformability, the capture efficiency was reported to be 70%, with the capability of processing 7.5 mL of whole blood of metastatic colorectal cancer patients using two chips.

Zhang et al. combined filtration and immune affinity principle for CTC retrieval in one platform to increase the isolation efficiency.[169] They presented a two-stage integrated microfluidic chip for CTC isolation from a whole blood sample. A novel release mechanism was developed based on air-liquid interfacial tension, which was used to peel off the membrane after blood cells had been extracted by filtering using a micropore-array membrane. The second stage involved a dense immunomagnetic bead clump for CTCs and provided a recovery rate of 86% and a purity of 38% for rare lung cancer cells (A549) spiked into whole blood.

As a different strategy for CTC clusters, Kamyabi et al. developed trap chambers relying on size differences and dynamic force balance in the trapped chamber.[170] This filter system lets blood cells and single CTCs pass but traps CTC clusters. ≈10 000 trap chambers were fabricated to isolate CTC clusters from the whole blood samples in 1 h. The collected CTC clusters were isolated with a backflush for further downstream analysis. The reported capture efficiency was 66–87%, and the release efficiency was between 76% and 90%, depending on the concentrations of clusters (Figure 3D).

CTCs from various types of cancer, especially CTC clusters, are larger and less deformable than leukocytes, which allows their isolation through filtration (e.g., microgaps, microposts, or gaps in the structure) from blood. Despite the advantages of filtration-based isolation, that is, cost-effectiveness and simple operation, traditional filters also have significant drawbacks, such as being less effective for isolating small and singular CTCs[162,171,172] and difficulties in retrieving collected CTCs and failures due to pore-clogging.[172–174]

4.2.3. Acoustophoresis-Based Isolation

Acoustophoresis relies on acoustic streaming and radiation forces. These forces act on suspended particles to achieve separation based on their physical and mechanical properties of the particles.

Acoustophoresis uses an acoustic pressure gradient within the channel, generating an acoustic radiation force that operates independently of pH, surface charge, or ionic strength, while preserving the integrity of particles or cells.[138,175] When an acoustic radiation force is applied, particles or cells move under the influence of ultrasound, which is determined by their size, density, and compressibility.[138] The standard approach to generate acoustic waves involves using piezoelectric transducers.

The acoustic force can vary significantly depending on the mechanical properties of the cell and the surrounding fluid (such as density and compressibility). Other forces acting on the cells include fluid shear forces, gravitational forces, and buoyant forces (**Figure 4**A). This results in cells being pushed toward a pressure node, where the periodic pressure variation is zero, or toward an anti-pressure node, where the acoustic pressure is maximal.[176] The migration duration and final position of cells within and after the acoustic field are influenced by the magnitude of acoustic radiation forces experienced by cells with varied volume, density, or compressibility values.[175]

Olm et al. utilized a peripheral blood progenitor cell (PBPC) suspension, spiked with transplant-contaminating neuroblastoma cells (NBCs), and introduced this sample to a microfluidic chip at a flow rate of 100 μL min^{-1}. The cells formed two parallel bands in the prealignment channel, which was controlled at 5 MHz by a resonator. A sorting buffer was supplied at a flow rate of 300 μL min^{-1} to enhance separation resolution, Aligned cells then entered a separation channel, where a second acoustic field influenced their lateral positioning based on their acoustic characteristics. Tumor cells experienced stronger radiation forces than the smaller blood cells, which caused them to move toward the center of the channel, while mononuclear cells (MNCs/PBPCs) exited through side outlets (Figure 4B).[177]

Lu et al. presented a platform that uses an array of microtraps combined with acoustic streaming to isolate breast cancer cell lines, achieving isolation efficiency of 95 ± 5% in spiked diluted serum and 66 ± 4% in whole blood samples. Each microtrap served as an active point to attract and hold surrounding cancer cells when ultrasound was applied, enabling size-based separation and discrimination of microparticles (Figure 4C).[178] Li et al. demonstrated the use of tilted interdigital transducers (IDTs) placed around a microfluidic channel to apply sound waves.[179] The generated acoustic radiation force (F_{ac}) acting on CTCs was greater than that (F_{aw}) acting on WBCs due to their larger size. As a result, CTCs had a larger vertical displacement than WBCs. No separation was observed when HeLa cancer cells and WBCs were mixed without an acoustic field. However, HeLa cells were collected at the outlet with the acoustic field activated, while WBCs remained in the waste outlet (Figure 4D).

Undvall Anand et al. introduced a novel two-step acoustophoresis platform designed for isolating DU145 cells from RBC-lysed whole blood.[180] The first step involved an acoustofluidic preseparation to separate cells based on their sonic mobility. It aimed to collect viable DU145 cells in the central outlet and WBCs in the side outlets. Due to the overlap in acoustophysical properties of these viable cells, a second step was necessary to eliminate WBC contamination by using negative selection acoustophoresis. The recovery rate of viable cancer varied between 28 and 42% depending on the concentration of cancer cells. The primary advantage of this platform is the ability to obtain viable cells for further analysis, although the recovery ratio remains minimal (Figure 4E).

One of its key advantages is its noncontact nature and the ability to isolate CTCs without applying mechanical forces, making it suitable for preserving cell viability in comparison to size-based label-free techniques. Since the technique is an active separation method, it also allows for tunable separation. CTC sizes in different cancer stages are reportedly different,[181] and this technique can be adapted to size changes during the operation. However, its limitations include challenges in separating CTCs from normal blood cells with similar or overlapping acoustic properties,[180] especially when CTCs exhibit heterogeneity in size or stiffness. Moreover, the resolution of acoustophoresis can

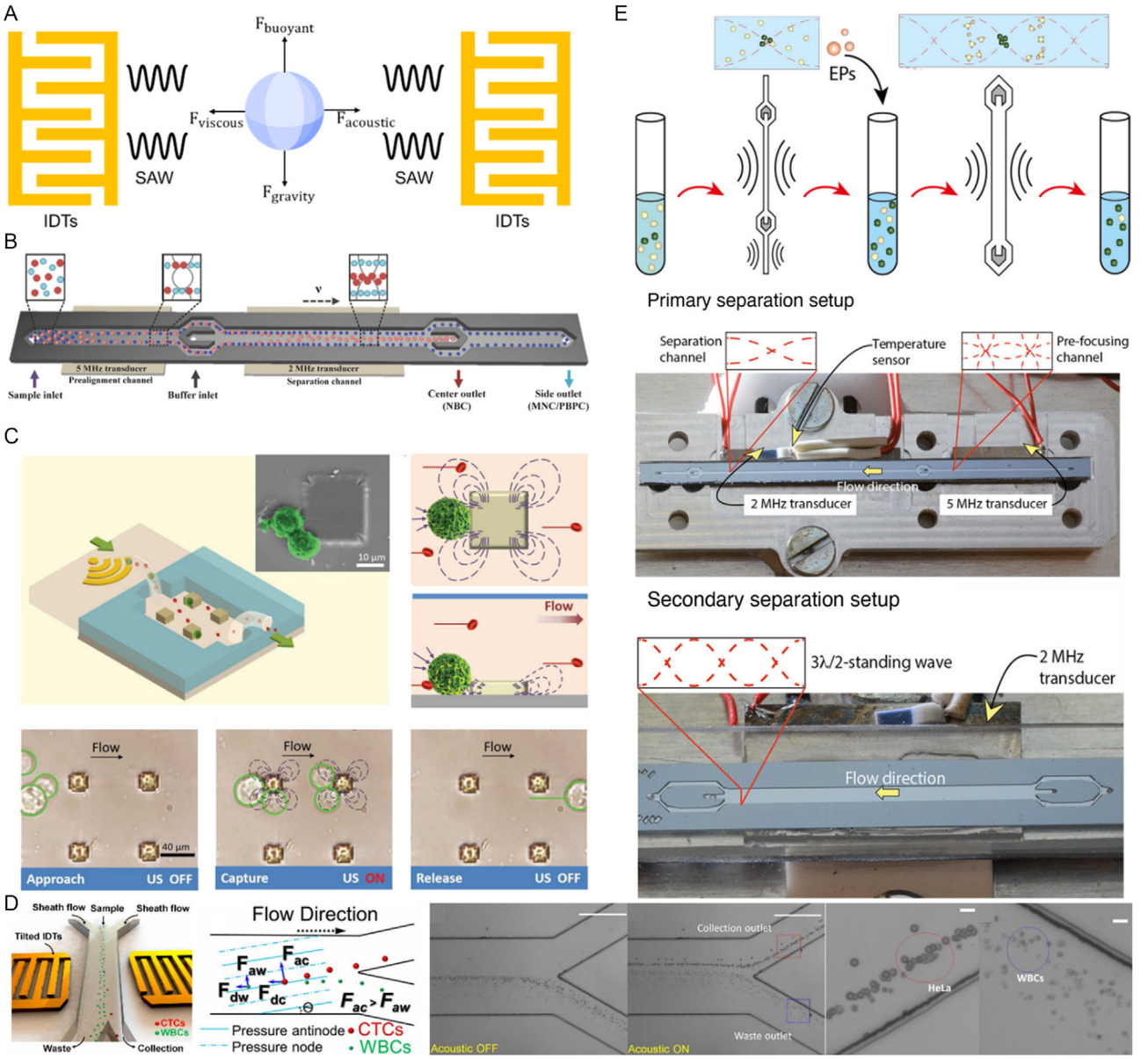

Figure 4. The working principle of acoustophoresis-based isolation. A) Diagrammatic representation of the various forces acting on a particle ($F_{acoustic}$ is the force created by an acoustic field generated by IDTs, $F_{viscous}$ is the shear force exerted by the liquid inside the microchannel, $F_{buoyant}$ is the upward force exerted by the liquid opposing the gravitation leading to floating of the particle inside the liquid, and $F_{gravity}$ is the gravitational force). Reproduced with permission.[138] Copyright 2019, Elsevier. B) Illustration of a two-stage acoustophoresis chip for NBC isolation. Reproduced under terms of the CC-BY license.[177] Copyright 2019, Olm et al. published by Springer Nature. C) Diagram of a parallel isolation microdevice for separating cancer cells (green) from a large number of RBCs in a biological fluid (red) (inset SEM of cancer cells that were trapped in a microtrap, scale bar: 10 mm). The top, bottom, and side perspectives of traps demonstrate how the acoustic capturing force produced by the trap can be used to isolate cancer cells based on their size. Actual microscopy images represent the flow of the cells (scale bar: 40 μm). Reproduced with permission.[178] Copyright 2018, John Wiley and Sons. D) Representation of tilted-angle standing surface acoustic waves (taSSAW)-based cell separation and working mechanism. Reproduced by permission.[179] Copyright 2015, Li et al. published by National Academy of Sciences. E) Illustration of the workflow of two-stage separation, the image of primary separation setup including aluminum chip holder before construction, secondary separation channel with two piezoelectric transducers for producing sound, and a temperature sensor. Reproduced under terms of the CC-BY license.[180] Copyright 2021, Undvall Anand et al. published by American Chemical Society.

be hindered by the complexity of the cellular environment in cancer patients, where the presence of high cell density may reduce efficiency. Therefore, a RBC lysis solution is often utilized to enhance the efficiency.[179,182] Since the RBC lysis solution has no adverse effects on CTCs, the only drawback of this step can be considered as increased processing time.[179]

4.2.4. DEP-Based Isolation

DEP is often used for cell sorting or isolation. DEP describes the movement of a polarizable particle in a nonhomogeneous electric field.[183] The movement is caused by the action of the nonhomogeneous field on the induced dipole in the cell. The force acting on the cells depends on the gradient of the electric field vector, the cell's volume, and the cell's relative polarizability in the medium, commonly expressed through the real part of the Clausius–Mossotti (CM) factor, Re[*CM*]. Re[*CM*] is frequency-dependent and bound between −0.5 and 1.0. If Re[*CM*] is negative, cells move against the field gradient towards regions of low electric field, termed negative DEP (nDEP) (**Figure 5**A). If Re[*CM*] is positive, cells move along the gradient, towards the local maximum of the electric field, termed positive DEP (pDEP).

Cells may experience pDEP or nDEP depending on excitation frequency and cell composition (Figure 5B).[184] Generally, the Re[*CM*] of a viable cell is negative at low field frequencies (below 10 kHz) and positive at intermediate to high field frequencies (up to several tens of MHz). The first crossover frequency depends on the cellular membrane's capacitance. Most DEP separators operate by exploiting differences in the first crossover frequency. It was shown that cancer cells have a significantly different first crossover frequency compared to blood cells.[185] Cancer cells have a higher membrane capacitance, due to their higher membrane folding factor (ϕ) than blood cells.[186] The "folding factor" is the ratio between the effective membrane area and the area of a sphere having the equivalent volume. Furthermore, variations in protein concentration, glycosylation, and changes in the cytoskeleton all influence the effective membrane capacitance.

Different approaches exist to generate the field inhomogeneity required for particle manipulation. The two main approaches are electrode-based DEP (eDEP)[187,188] and insulator-based DEP (iDEP).[189,190] In eDEP, the field inhomogeneity comes from the electrodes' asymmetry. The most common approach is an array of interdigitated microelectrodes positioned at the bottom of a microfluidic chip. The resulting electric field will be strongest close to the electrodes and decreases with distance from the array. Because the DEP force drops with distance from the array, 3D concepts exist to obtain a more homogeneous distribution of the DEP force in the channel. In iDEP, the electrodes are positioned outside of the actual separation regions. The electric field gradient is then generated by scattering the superimposed electric field at insulating posts or obstacles positioned in the separation region.

Two main strategies exist to isolate target particles from a mixture of target and nontarget particles,[191] that is, to isolate CTCs from whole blood or buffy coat. The first option is to isolate cells by selective immobilization in local field maxima; this is usually referred to as trapping. For this, the target cells need to experience a sufficiently large pDEP force that is strong enough to act against fluidic drag forces, whereas nontarget cells should either experience nDEP or only weak pDEP. Target cells remain isolated until the field is turned off. This allows semibatch operation with alternating trapping and release steps. The second option for cell isolation is to sort target and nontarget cells into different outlets on a microfluidic chip. The main requirement is that the DEP force between target and nontarget particles must be sufficiently different to move both particle types onto different streamlines that either lead to different outlets or elute at different times from the device. Both approaches can be implemented with either iDEP or eDEP setups. The approaches are also called nonequilibrium (trapping) and equilibrium (sorting) approaches and have been discussed by Gascoyne and Shim.[192]

Here, we highlight a few selected DEP applications for isolating CTC from blood samples. This list is not necessarily exhaustive. One notable device is ApoStream, a commercially available cell-sorting system marketed by Precision for Medicine.[193] It is promoted as a label-free sorter of CTCs from blood and is based on earlier dielectrophoretic field-flow fraction techniques for isolating rare cells.[185,188,194,195] The device consists of a large interdigitated electrode array located at the bottom of the device. Samples are injected through a port at the bottom in front of the electrode array, while an elution buffer is continuously flushed through a second port, reducing the sample's conductivity. For selective DEP separation to be successful, the conductivity of the medium must be significantly lower (about 30–60 mS m^{-1}) compared to that of physiological media (1.6 S m^{-1}). After entering the device, all cells initially gather close to the electrode array. At the appropriate frequency, CTCs experience a pDEP, allowing them to remain near the electrode array (but not become trapped), while peripheral blood mononuclear cells (PBMCs) experience a nDEP and are pushed away to other streamlines. CTCs, positioned on streamlines near the electrodes, are directed toward a collection outlet at the bottom, while PBMCs, on higher streamlines, are diverted to a waste outlet and discarded. In benchmark experiments,[193] ApoStream successfully processed 12×10^6 PBMCs (equivalent to 7.5 mL of blood) in 60 min. It recovered both SKOV3 ovarian and MDA-MB-231 breast cancer cells spiked into PBMCs from healthy donors at concentrations as low as 4 cells per 12×10^6 cells. SKOV3 is an ovarian cancer cell line with high EpCAM expression, while MDA-MB-231 exhibits low EpCAM expression. The experiments demonstrated recovery efficiencies ranging from 50% to ≈75% for both cell types without losing cell viability after isolation.

In a subsequent study, Balasubramanian et al.[196] conducted a crosslaboratory validation of ApoStream through spike-recovery experiments with cancer cells from three different phenotypes (MDA-MB-231 breast cancer, A549 lung adenocarcinoma cell, and ASPS-1 sarcoma). They spiked 1000 or 50 cells into 10^7 PBMCs in 1 mL of the sample. They observed 68% and 55% mean recovery rates for the higher and lower spiking levels, respectively. The lower recovery rates at lower spiking levels were attributed to inherent cell loss inside tubings, flow chambers, and pipette tips. Additionally, they noted that, of the 10^7 PBMCs present at the input, about 6000–35 000 were found in the single-pass purified sample, depending on the applied field frequency. The required field frequency also varied based on cancer cell phenotype. The authors performed tests on blood samples from six patients with alveolar soft part sarcoma (ASPS). They successfully recovered CTCs from all six patients, as demonstrated by a transcription factor binding to IGHM enhancer 3 break-apart fluorescent in situ hybridization analysis. Importantly, they demonstrated that using parameters derived from cell-line experiments enabled successful isolation of CTCs from clinical samples, achieving a performance comparable to that expected from spike-recovery experiments.

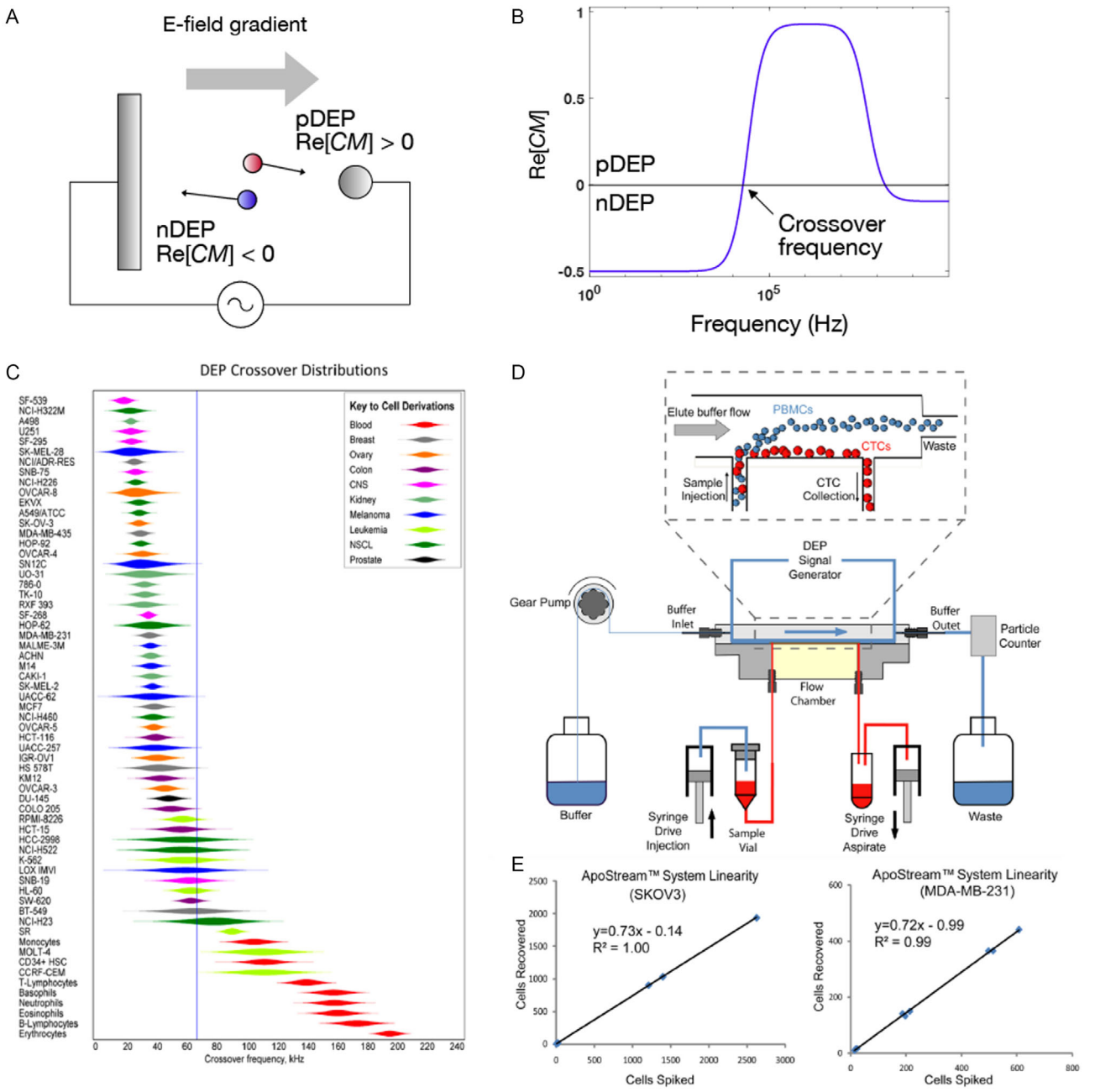

Figure 5. The working principle of DEP-based isolation. A) Particles or cells move to electric field maxima when they experience pDEP conversely; they move to the electric field minima when they experience nDEP. B) The real part of the Clausius–Mossotti factor decides the strength and direction of the DEP force. Cells usually have a negative Re[*CM*] at low frequencies and experience a crossover from negative to positive at a frequency between 10 and 100 kHz (termed first crossover frequency). C) Common cancer cell lines (NCI-60 panel) have a first crossover frequency that is significantly lower than blood cells. This allows separation by DEP. Reproduced with permission.[185] Copyright 2013, AIP Publishing. D) ApoStream system working principle. Reproduced with permission.[193] Copyright 2012, AIP Publishing. E) ApoStream system linearity and recovery rates are shown for two cancer cell lines, SKOV3 and MDA-MB231. Reproduced with permission.[193] Copyright 2012, AIP Publishing.

Other researchers utilized ApoStream to recover CTCs from clinical samples of patients with various metastatic cancers to detect folate receptor alpha $(FR\alpha)^+$ cells.[197] Le Du et al.[198] used ApoStream to recover CTCs and identify subsets (E-CTC, E/M-CTC, M-CTC, and cancer stem-like cells, CSC) from breast cancer patients at different treatment stages. Although they could not correlate the CTC counts to pathological complete response (pCR), this study emphasized the importance of marker-independent cancer cell isolation, as E/M-CTCs, M-CTCs, and CSCs cannot be captured using EpCAM-specific isolation strategies.

Other dielectrophoretic methods for identifying CTCs also exist. For instance, Henslee et al.[199] used contactless DEP (cDEP), a variant of iDEP where the electrodes are separated from the separation area by a thin insulating membrane, to separate normal MCF10A breast cells, MCF-7 luminal breast cancer cells, and MDA-MB-231 TNBC cells. They argued that these human breast cells represent early, intermediate, and late-stage breast cancer, respectively. Without focusing on target-cell concentration or throughput, the authors successful isolated MDA-MB-231 cells from a population containing MCF10A and MCF-7 cells when operating at 30 V_{rms} and 164 kHz. In a later feasibility study,[200] cDEP was utilized to separate tumor subpopulations, namely highly aggressive MOSE-L_{TICv} cells from the less aggressive MOSE-L mouse ovarian surface epithelial cells, both derived from the same MOSE-L cell line. The authors suggested that their experiments could be an in vitro models mimicking expected in vivo behavior.

Additionally, Bhattacharya et al.[190] conducted feasibility analyses using iDEP, successfully trapping individual MCF-7 cells in a mixed population of MCF-7 and PBMCs and a mixed population of MCF-7 and MDA-MB-231 cells. Li and Anand[201] used wireless electrodes, also sometimes called floating electrodes, to separate MDA-MB-231 from Jurkat E6-1 leukemic cells; the authors use the latter as a model for T cells. Specifically, the authors demonstrated single-cell capture of target cells and suggested that their device is easily scalable, allowing them to reach clinically relevant throughputs comparable to ApoStream. Unlike ApoStream, single cells were isolated on the chip, allowing for easy downstream on-chip analysis. Cheng et al.[202] used 3D, V-shaped electrodes to move CTCs lateral to the flow direction. They separated PC14PE6/AS2 green fluorescent protein (GFP)-labeled human lung adenocarcinoma cells spiked into white and RBCs at different ratios from 1:10 000 to 1:500 000. The authors achieved an 85% recovery rate at a throughput of 1.2 mL h^{-1}. However, final cell concentrations were around two orders of magnitude lower than expected in clinical samples.

Huang et al. used optical DEP to separate prostate cancer (PC-3) cells and human oral cancer (OEC-M1) spiked into a leukocyte population. Optical DEP works by applying a homogeneous electric field across a trapping region. One electrode is coated with a thin photoconductive material. If the photoconductive layer is illuminated, its impedance drops locally, thus creating a local inhomogeneous electric field. This method avoids complicated microelectrode fabrication. Their method was able to isolate PC-3 and OEC-M1 cells from a leukocyte background with a high recovery rate of 76–83% (PC-3) and 61–68% (OEC-M1). They also achieved a high purity (PC-3 cells: 74–82%, OEC-M1 cells: 64–66%) at a set flow rate of 0.1 µL min^{-1} and sample volume of 1 µL.

DEP is unique as a sorting method because the dependence of the polarizability on the membrane capacitance allows the discrimination of cells by properties that are not accessible by other techniques. It allows for the separation of CTCs from blood cells, even if they are the same size as blood cells, if their size changes depending on the cancer stage,[181] or if they do not express different surface markers. This is because malignant cells show different glycosylation and phosphorylation of the membrane proteins.[184] In addition, several researchers demonstrated that DEP could distinguish between different cell lines derived from the same tissue, for example, MCF-7 breast cancer cells and MCF10A breast cells, based on dielectric property differences.[199,203] Therefore, this technique becomes particularly advantageous for isolating CTCs in heterogeneous populations.[204]

There are good reviews that discuss the strengths and weaknesses of DEP for cancer cell isolation.[184,192,205] While DEP has access to unique cell properties for isolation, it also suffers from some drawbacks. One challenge is carefully optimizing of the applied electric field to accommodate the diversity of CTCs, which is required,[206] since cell type, size, membrane characteristics, and morphology variations can affect CTCs' response to the field. Besides, a presuspending step is often necessary, which is the process of transferring the cells in an iso-osmolar low-conductivity medium.[207,208] Another challenge is the achievable throughput, especially considering the low concentration of target cells in the blood. DEP is mainly a microfluidic technique; while many studies present thoughtful advances on increasing selectivity, fewer papers demonstrate clinically relevant throughputs. A third challenge is the transfer from model systems (i.e., experiments with cell lines) to clinical samples. As discussed by Shim et al.[188] dielectrophoretic properties of the blood of cancer patients are modified by the disease and treatment. This might cause the presence of blood cell subpopulations that can negatively impact the CTC isolation. An ongoing concern is the ion leakage and decrease in cell viability caused by the presence of strong electric fields applied for cell isolation, which was reported by Menachery et al.[209] and Gascoyne et al.[192]

4.3. Automated and Integrated Platforms for Efficient CTC Isolation

Compared to other isolation platforms like density-gradient centrifugation, microfluidic-based isolation is preferred for various applications due to its low sample consumption, rapid processing times, ease of automation, high throughput, and overall efficiency. However, there is often a compromise between efficiency and throughput.[210]

A literature study introduced a DLD-based microfluidic system integrated with an automatic purification device using CD45-labeled immunomagnetic beads and a capturing platform coated with rat-tail collagen.[211] This system enables the rapid and sensitive identification of CTCs. Furthermore, another recent study developed an automated system combining a 3D printed off-chip multisource reagent platform, an air-bubble retainer, and a single CTC-capturing microchip. This system can successfully capture and identify CTCs in less than 90 min. In contrast to conventional CTC identification techniques, this technology performs immunoassays on-chip with full automation, reducing immunostaining time and antibody consumption by 90%.[212]

A notable trend in microfluidics is the integration of artificial intelligence (AI), machine learning (ML), and deep learning (DL) into CTC isolation platforms. Einoch-Amor et al. combined AI with nanoarrays to detect CTCs specifically using A549 lung cancer cells spiked into blood samples.[11] Another recent study developed a precise and fast image-processing algorithm using convolutional neural networks (CNN) to detect CTCs in patients with esophageal squamous cell carcinoma (ESCC). Researchers

assessed the algorithm's accuracy in differentiating ESCC cell lines from PBMCs and subsequently applied it to identify CTCs in blood samples from ESCC patients. The average time to complete cell classification for 100 images was 0.74 s for the AI and 630.4 s for the researchers, with a statistical significance of $P = 0.012$. The accuracy of distinguishing esophageal cancer cell lines (KYSE series) from PBMCs in the same study was 100% for AI and 92% for the researchers.[213] The integration of AI-based technologies for CTC isolation and characterization is expected to open a new era of automated detection of CTCs' phenotypes and genotypes, enhancing screening and analysis in a high-throughput manner.[11] Additionally, a novel approach involving bioimprinting technology has been developed for the label-free isolation of pancreatic tumor cells. In this protocol, cells are imprinted on functionalized polymers to create specific spaces, allowing for preferential retention of targeted cancer cells from PBMCs.[214]

5. Conclusion and Future Perspectives

The isolation and characterization of CTCs as a biomarker in liquid biopsy has great promise to improve cancer diagnosis, determine prognosis, and monitor the effectiveness of cancer treatment. CTCs are rare among blood cells; they possess phenotypic heterogeneity and size variations, and often, it is required to maintain their viability for downstream functional analysis. Therefore, more efforts are needed to improve CTC isolation platforms. Recent advancements in microfluidic technologies offer great potential to address the limitations and to improve throughput, purity, recovery, and clinical relevance.

Microfluidic devices exploit differences in the physical (size, electrical charge, etc.) and biological properties (cell receptor affinity) of cells, independently or in combination. Label-free strategies might enable a higher yield than the current affinity-based techniques, since affinity-based techniques require markers like EpCAM. The heterogeneous nature of CTCs, such as those influenced by EMT, leads to the downregulation of epithelial markers like EpCAM, thereby reducing the capture yield of CTCs. Efficiently isolating heterogeneous CTCs using label-free methods could significantly enhance clinical applications, including earlier detection of aggressive tumors, improved therapy selection, and better detection of drug resistance, as well as the ability to identify novel therapeutic targets.

Label-free microfluidic technology relies on various particle separation techniques. This review extensively discussed four primary methods, focusing on their mechanism and efficiency in isolating heterogeneous CTCs.

Considerable progress has been made in the use of microfluidic devices in clinical trials, and several commercially available technologies now utilize label-free separation. Currently, there are platforms available for both label-free and label-based CTC isolation. For example, CanPatrol^{TM} system utilizes an affinity-based isolation technique similar to CellSearch. Label-free commercial products include filtration methods such as ISET (Isolation by SizE of Tumor cells; Rarecells diagnostics), MetaCell, and ScreenCell, as well as size-based separation technologies like Parsortix (Angle plc) and ClearCell FX1 (Clearbridge Biomedics), and DEP methods including ApoStream (Apocell, Inc.) and DEPArray (Menarini Silicon Biosystems).

This review highlights the significant potential of CTCs in prognostication and particularly emphasizes the critical need for efficient and straightforward CTC isolation methodologies. Combining functional and molecular characterization of CTCs with isolation techniques allows for a deeper understanding of disease conditions. Further research into CTC isolation methods is necessary to efficiently capture all types of CTCs from whole blood. Characterizing the various types of cells is essential for monitoring cancer progression and treatment efficacy, as they collectively provide important clinical information about tumor stages.[3] Given that CTC analysis has shown considerable promise and delivers critical insights in preclinical models, microfluidic-based isolation devices should aim to achieve superior sorting efficiency in clinical studies. Additionally, these devices should be compatible with current downstream characterization procedures and should integrate DL, ML, and AI into diagnostics while providing high-throughput isolation capabilities.

Acknowledgements

This work is funded by the Netherlands Organization for Health Research and Development (ZonMw): 09120012010061. The authors are grateful to the laboratory team members for valuable discussion. GÖ and ED contributed equally to this work. The present address of ED is "Department of Biosystems Science and Engineering, ETH Zurich, 4056 Basel, Switzerland". Figure 1A,B was made in BioRender.com.

Conflict of Interest

The authors declare no conflict of interest.

Author Contributions

Gürhan Özkayar: writing—original draft (lead); validation (equal). **Esma Derin**: writing—original draft (equal); validation (lead). **Georg R. Pesch**: supervision (supporting); writing—review and editing (supporting); validation (supporting). **John W. M. Martens**: funding acquisition: (supporting); writing—review and editing (supporting). **Peter ten Dijke**: funding acquisition (lead); supervision (supporting); writing—review and editing (supporting). **Pouyan E. Boukany**: conceptualization (lead); funding acquisition (supporting); supervision (lead); writing—review and editing (lead).

Keywords

cancer cell heterogeneities, circulating tumor cells, epithelial-to-mesenchymal transitions, label-free isolations, microfluidics

Received: November 15, 2024
Revised: March 3, 2025
Published online: May 8, 2025

[1] WHO, *"Cancer"*, https://www.who.int/news-room/fact-sheets/detail/cancer, (accessed: March, 2025).
[2] WHO, "Overview: *Cancer*", https://www.who.int/health-topics/cancer#tab=tab_1, (accessed: March, 2025).

[3] S. Sharma, R. Zhuang, M. Long, M. Pavlovic, Y. Kang, A. Ilyas, W. Asghar, *Biotechnol. Adv.* **2018**, *36*, 1063.
[4] S. Chen, Z. Cao, K. Prettner, M. Kuhn, J. Yang, L. Jiao, Z. Wang, W. Li, P. Geldsetzer, T. Bärnighausen, et al., *JAMA Oncol.* **2023**, *9*, 465.
[5] National Cancer Institute, "*Liquid Biopsy*", https://www.cancer.gov/publications/dictionaries/cancer-terms/def/liquid-biopsy, (accessed: March, 2025).
[6] T. H. Visal, P. den Hollander, M. Cristofanilli, S. A. Mani, *Br. J. Cancer* **2022**, *127*, 173.
[7] A. M. Sieuwerts, J. Kraan, J. Bolt, P. Van Der Spoel, F. Elstrodt, M. Schutte, J. W. M. Martens, J. W. Gratama, S. Sleijfer, J. A. Foekens, *J. Natl. Cancer Inst.* **2009**, *101*, 61.
[8] K. C. Andree, G. van Dalum, L. W. M. M. Terstappen, *Mol. Oncol.* **2016**, *10*, 395.
[9] J. F. Swennenhuis, G. Van Dalum, L. L. Zeune, L. W. M. M. Terstappen, G. Van Dalum, L. L. Zeune, L. W. M. M. Terstappen, *Expert Rev. Mol. Diagn.* **2016**, *16*, 1291.
[10] M. M. Ferreira, V. C. Ramani, S. S. Jeffrey, *Mol. Onco.l* **2016**, *10*, 374.
[11] R. Einoch-Amor, Y. Y. Broza, H. Haick, *ACS Nano* **2021**, *15*, 7744.
[12] M. D. Tarn, N. Pamme, *Reference Module in Chemistry, Molecular Sciences and Chemical Engineering*, Elsevier, Amsterdam, The Netherlands **2014** Ch. Microfluidics.
[13] Z. Zhang, S. Nagrath, *Biomed. Microdevices* **2013**, *15*, 595.
[14] S. Kumari, U. Saha, M. Bose, D. Murugan, V. Pachauri, V. V. R. Sai, N. Madaboosi, *Chemosensors* **2023**, *11*, 107.
[15] H. Esmaeilsabzali, T. V. Beischlag, M. E. Cox, A. M. Parameswaran, E. J. Park, *Biotechnol. Adv.* **2013**, *31*, 1063.
[16] Z. Eslami-S, L. E. Cortés-Hernández, C. Alix-Panabières, *Cells* **2020**, *9*, 1836.
[17] Z. Deng, S. Wu, Y. Wang, D. Shi, *EBioMedicine* **2022**, *83*, 104237.
[18] J. Dong, J. F. Chen, M. Smalley, M. Zhao, Z. Ke, Y. Zhu, H. R. Tseng, *Adv. Mater.* **2020**, *32*, 1903663.
[19] H. Pei, L. Li, Z. Han, Y. Wang, B. Tang, *Lab Chip* **2020**, *20*, 3854.
[20] H. Cho, J. Kim, H. Song, K. Y. Sohn, M. Jeon, K. H. Han, *Analyst* **2018**, *143*, 2936.
[21] L. Descamps, D. Le Roy, A. L. Deman, *Int. J. Mol. Sci.* **2022**, *23*, 1981.
[22] J. F. Edd, A. Mishra, K. C. Smith, R. Kapur, S. Maheswaran, D. A. Haber, M. Toner, *iScience* **2022**, *25*, 1.
[23] S. J. Hao, Y. Wan, Y. Q. Xia, X. Zou, S. Y. Zheng, *Adv. Drug Deliv. Rev.* **2018**, *125*, 3.
[24] C. Jin, S. M. McFaul, S. P. Duffy, X. Deng, P. Tavassoli, P. C. Black, H. Ma, *Lab Chip* **2014**, *14*, 32.
[25] B. Michela, *Diagnostics* **2021**, *11*, 1391.
[26] G. Siravegna, S. Marsoni, S. Siena, A. Bardelli, *Nat. Rev. Clin. Oncol.* **2017**, *14*, 531.
[27] S. Keller, J. Ridinger, A. K. Rupp, J. W. G. Janssen, P. Altevogt, *J. Transl. Med.* **2011**, *9*, 86.
[28] C. Lässer, *Methods Mol. Biol.* **2013**, *1024*, 109.
[29] M. E. Menyailo, M. S. Tretyakova, E. V. Denisov, *Int. J. Mol. Sci.* **2020**, *21*, 1696.
[30] S. C. P. Williams, *Proc. Natl. Acad. Sci. U. S. A.* **2013**, *110*, 4861.
[31] M. Han, J. A. Watts, A. Jamshidi-Parsian, U. Nadeem, M. Sarimollaoglu, E. R. Siegel, V. P. Zharov, E. I. Galanzha, *Cancers* **2020**, *12*, 1.
[32] C. Macaraniag, Q. Luan, J. Zhou, I. Papautsky, *APL Bioeng.* **2022**, *6*, 031501.
[33] C. Paoletti, J. Miao, E. M. Dolce, E. P. Darga, M. I. Repollet, G. V. Doyle, J. R. Gralow, G. N. Hortobagyi, J. B. Smerage, W. E. Barlow, et al., *Clin. Cancer Res.* **2019**, *25*, 6089.
[34] I. Fridrichova, L. Kalinkova, S. Ciernikova, *Int. J. Mol. Sci.* **2022**, *23*, 12141.
[35] S. Chai, N. Matsumoto, R. Storgard, C. C. Peng, A. Aparicio, B. Ormseth, K. Rappard, K. Cunningham, A. Kolatkar, R. Nevarez, et al., *Mol. Cancer Res.* **2021**, *19*, 2036.
[36] N. Aceto, A. Bardia, D. T. Miyamoto, M. C. Donaldson, B. S. Wittner, J. A. Spencer, M. Yu, A. Pely, A. Engstrom, H. Zhu, et al., *Cell* **2014**, *158*, 1110.
[37] Z. Hu, Z. Li, Z. Ma, C. Curtis, *Nat. Genet.* **2020**, *52*, 701.
[38] Y. Chen, X. Du, A. Kuppa, M. F. Feitosa, L. F. Bielak, J. R. O'Connell, S. K. Musani, X. Guo, B. Kahali, V. L. Chen, et al., *Nat Genet* **2023**, *55*, 1640.
[39] L. Xu, X. Mao, A. Imrali, F. Syed, K. Mutsvangwa, D. Berney, P. Cathcart, J. Hines, J. Shamash, Y. J. Lu, *PLoS One* **2015**, *10*, e0138032.
[40] Q. Li, S. Cui, Y. Xu, Y. Wang, F. Jin, H. Si, L. Li, B. Tang, *Anal. Chem.* **2019**, *91*, 14133.
[41] G. Özkayar, E. Mutlu, Ş. Şahin, Y. D. Yalçın, T. Töral, H. Külah, E. Yıldırım, Ö. Zorlu, E. Özgür, *Micromachines* **2020**, *11*, 981.
[42] I. Dagogo-Jack, A. T. Shaw, *Nat. Rev. Clin. Oncol.* **2018**, *15*, 81.
[43] C. E. Meacham, S. J. Morrison, *Nature* **2013**, *501*, 328.
[44] D. R. Caswell, C. Swanton, *BMC Med.* **2017**, *15*, 133.
[45] P. R. Prasetyanti, J. P. Medema, *Mol. Cancer* **2017**, *16*, 1.
[46] G. Turashvili, E. Brogi, *Front. Med.* **2017**, *4*, 227.
[47] A. Gavish, M. Tyler, A. C. Greenwald, R. Hoefflin, D. Simkin, R. Tschernichovsky, N. Galili Darnell, E. Somech, C. Barbolin, T. Antman, et al., *Nature* **2023**, *618*, 598.
[48] K. Andrade de Oliveira, S. Sengupta, A. K. Yadav, R. Clarke, *Front. Endocrinol.* **2023**, *14*, 1083048.
[49] T. Yu, C. Wang, M. Xie, C. Zhu, Y. Shu, J. Tang, X. Guan, *Biomed. Pharmacother.* **2021**, *137*, 111314.
[50] L. Guo, D. Kong, J. Liu, L. Zhan, L. Luo, W. Zheng, Q. Zheng, C. Chen, S. Sun, *Exp. Hematol. Oncol.* **2023**, *12*, 3.
[51] D. Marrinucci, K. Bethel, A. Kolatkar, M. S. Luttgen, M. Malchiodi, F. Baehring, K. Voigt, D. Lazar, J. Nieva, L. Bazhenova, et al., *Phys. Biol.* **2012**, *9*, 016003.
[52] C. Agnoletto, F. Corrà, L. Minotti, F. Baldassari, F. Crudele, W. J. J. Cook, G. Di Leva, A. P. D'Adamo, P. Gasparini, S. Volinia, *Cancers* **2019**, *11*, 9.
[53] Y. Hou, J. Lin, H. Yao, Z. Wu, Y. Lin, J. Lin, *Adv. Sci.* **2025**, 2413978.
[54] M. Tellez-Gabriel, M. F. Heymann, D. Heymann, *Theranostics* **2019**, *9*, 4580.
[55] Z. Habli, W. Alchamaa, R. Saab, H. Kadara, M. L. Khraiche, *Cancers* **2020**, *12*, 1.
[56] F. Bin Hamid, V. Gopalan, M. Matos, C. T. Lu, A. K. Y. Lam, *Int. J. Mol. Sci.* **2020**, *21*, 1.
[57] Z. Ahmed, S. Gravel, *Mol. Biol. Evol.* **2018**, *35*, 2135.
[58] J. Xu, K. Liao, X. Yang, C. Wu, W. Wu, S. Han, *Mol. Cancer* **2021**, *20*, 104.
[59] F. Rothé, D. Venet, D. Peeters, G. Rouas, M. Rediti, D. Smeets, F. Dupont, P. Campbell, D. Lambrechts, L. Dirix, et al., *NPJ Breast Cancer* **2022**, *8*, 79.
[60] C. Paoletti, A. K. Cani, J. M. Larios, D. H. Hovelson, K. Aung, E. P. Darga, E. M. Cannell, P. J. Baratta, C. J. Liu, D. Chu, et al., *Cancer Res.* **2018**, *78*, 1110.
[61] E. Pailler, N. Auger, C. R. Lindsay, P. Vielh, A. Islas-Morris-Hernandez, I. Borget, M. Ngo-Camus, D. Planchard, J. C. Soria, B. Besse, et al., *Ann. Oncol.* **2015**, *26*, 1408.
[62] S. L. Kong, X. Liu, S. J. Tan, J. A. Tai, L. Y. Phua, H. M. Poh, T. Yeo, Y. W. Chua, Y. X. Haw, W. H. Ling, et al., *Front. Oncol.* **2021**, *11*, 698551.
[63] L. R. Yates, M. Gerstung, S. Knappskog, C. Desmedt, G. Gundem, P. Van Loo, T. Aas, L. B. Alexandrov, D. Larsimont, H. Davies, et al., *Nat. Med.* **2015**, *21*, 751.

[64] A. Auwal, M. M. Hossain, T. U. H. Pronoy, K. M. Rashel, M. Nurujjaman, A. K. Y. Lam, F. Islam, *J. Liquid Biopsy* **2024**, *3*, 100135.
[65] A. A. Powell, A. A. H. Talasaz, H. Zhang, M. A. Coram, A. Reddy, G. Deng, M. L. Telli, R. H. Advani, R. W. Carlson, J. A. Mollick, et al., *PLoS One* **2012**, *7*, e33788.
[66] Q. Zhan, B. Liu, X. Situ, Y. Luo, T. Fu, Y. Wang, Z. Xie, L. Ren, Y. Zhu, W. He, et al., *Signal Transduct Target Ther.* **2023**, *8*, 465.
[67] B. Alberter, C. A. Klein, B. Polzer, *Expert Rev. Mol. Diagn.* **2016**, *16*, 25.
[68] T. M. Gorges, A. Kuske, K. Röck, O. Mauermann, V. Müller, S. Peine, K. Verpoort, V. Novosadova, M. Kubista, S. Riethdorf, et al., *Clin. Chem.* **2016**, *62*, 1504.
[69] J. Seo, M. Kumar, J. Mason, F. Blackhall, N. Matsumoto, C. Dive, J. Hicks, P. Kuhn, S. N. Shishido, *Sci. Rep.* **2023**, *13*, 11775.
[70] B. Bakir, A. M. Chiarella, J. R. Pitarresi, A. K. Rustgi, *Trends Cell Biol.* **2020**, *30*, 764.
[71] V. da Silva-Diz, L. Lorenzo-Sanz, A. Bernat-Peguera, M. Lopez-Cerda, P. Muñoz, *Semin Cancer Biol.* **2018**, *53*, 48.
[72] H. I. Scher, R. P. Graf, N. A. Schreiber, B. McLaughlin, A. Jendrisak, Y. Wang, J. Lee, S. Greene, R. Krupa, D. Lu, et al., *Cancer Res.* **2017**, *77*, 5687.
[73] A. S. McDaniel, R. Ferraldeschi, R. Krupa, M. Landers, R. Graf, J. Louw, A. Jendrisak, N. Bales, D. Marrinucci, Z. Zafeiriou, et al., *BJU Int.* **2017**, *120*, E30.
[74] A. Genna, A. M. Vanwynsberghe, A. V. Villard, C. Pottier, J. Ancel, M. Polette, C. Gilles, *Cancers* **2020**, *12*, 1.
[75] J. van Staalduinen, D. Baker, P. ten Dijke, H. van Dam, *Oncogene* **2018**, *37*, 6195.
[76] J. Yang, P. Antin, G. Berx, C. Blanpain, T. Brabletz, M. Bronner, K. Campbell, A. Cano, J. Casanova, G. Christofori, et al., *Nat. Rev. Mol. Cell Biol.* **2020**, *21*, 341.
[77] T. T. Onder, P. B. Gupta, S. A. Mani, J. Yang, E. S. Lander, R. A. Weinberg, *Cancer Res.* **2008**, *68*, 3645.
[78] A. Eger, A. Stockinger, J. Park, E. Langkopf, M. Mikula, J. Gotzmann, W. Mikulits, H. Beug, R. Foisner, *Oncogene* **2004**, *23*, 2672.
[79] H. hua Chen, X. long Zhou, Y. lu Shi, J. Yang, *Arch. Med. Res.* **2013**, *44*, 93.
[80] K.-A. Hyun, G.-B. Koo, H. Han, J. Sohn, W. Choi, S.-I. Kim, H.-I. Jung, Y.-S. Kim, *Oncotarget* **2016**, *7*, 24677.
[81] T. C. Brown, N. V. Sankpal, W. E. Gillanders, *Biomolecules* **2021**, *11*, 956.
[82] M. Santisteban, J. M. Reiman, M. K. Asiedu, M. D. Behrens, A. Nassar, K. R. Kalli, P. Haluska, J. N. Ingle, L. C. Hartmann, M. H. Manjili, et al., *Cancer Res.* **2009**, *69*, 2887.
[83] C. Y. Loh, J. Y. Chai, T. F. Tang, W. F. Wong, G. Sethi, M. K. Shanmugam, P. P. Chong, C. Y. Looi, *Cells* **2019**, *8*, 1118.
[84] A. Hollestelle, J. K. Peeters, M. Smid, M. Timmermans, L. C. Verhoog, P. J. Westenend, A. A. J. Heine, A. Chan, A. M. Sieuwerts, E. A. C. Wiemer, et al., *Breast Cancer Res. Treat.* **2013**, *138*, 47.
[85] Y. Wang, Y. Liu, L. Zhang, L. Tong, Y. Gao, F. Hu, P. P. Lin, B. Li, T. Zhang, *J. Cancer Res. Clin. Oncol.* **2019**, *145*, 2911.
[86] Y. Sun, G. Wu, K. S. Cheng, A. Chen, K. H. Neoh, S. Chen, Z. Tang, P. F. Lee, M. Dai, R. P. S. Han, *EBioMedicine* **2019**, *46*, 133.
[87] T. Rossi, G. Gallerani, G. Martinelli, R. Maltoni, F. Fabbri, *Biomedicines* **2021**, *9*, 1242.
[88] A. Ring, B. D. Nguyen-Sträuli, A. Wicki, N. Aceto, *Nat. Rev. Cancer* **2023**, *23*, 95.
[89] X. L. Zhang, P. P. Xie, K. T. Zhang, W. Zhang, *Cell. Oncol.* **2023**, *46*, 533.
[90] Q. Zhao, B. Li, Q. Gao, Y. Luo, L. Ming, *Front. Oncol.* **2022**, *12*, 1024783.
[91] Y. Huangfu, J. Guo, Y. Zhao, X. Cao, L. Han, *Cancer Manag. Res.* **2024**, *16*, 325.
[92] Y. Manjunath, S. V. Upparahalli, D. M. Avella, C. B. Deroche, E. T. Kimchi, K. F. Staveley-O'carroll, C. J. Smith, G. Li, J. T. Kaifi, *Cancers* **2019**, *11*, 806.
[93] M. Zeinali, M. Lee, A. Nadhan, A. Mathur, C. Hedman, E. Lin, R. Harouaka, M. S. Wicha, L. Zhao, N. Palanisamy, et al., *Cancers* **2020**, *12*, 127.
[94] A. J. Armstrong, M. S. Marengo, S. Oltean, G. Kemeny, R. L. Bitting, J. D. Turnbull, C. I. Herold, P. K. Marcom, D. J. George, M. A. Garcia-Blanco, *Mol. Cancer Res.* **2011**, *9*, 997.
[95] M. K. Jolly, S. A. Mani, H. Levine, *Biochim. Biophys. Acta Rev. Cancer* **2018**, *1870*, 151.
[96] M. Yu, A. Bardia, B. S. Wittner, S. L. Stott, M. E. Smas, D. T. Ting, S. J. Isakoff, J. C. Ciciliano, M. N. Wells, A. M. Shah, et al., *Science* **2013**, *339*, 580.
[97] B. Heitmeir, M. Deniz, W. Janni, B. Rack, F. Schochter, L. Wiesmüller, *Cancers* **2022**, *14*, 997.
[98] S. Anvari, E. Osei, N. Maftoon, *Sci. Rep.* **2021**, *11*, 15477.
[99] W. J. Allard, J. Matera, M. C. Miller, M. Repollet, M. C. Connelly, C. Rao, A. G. J. Tibbe, J. W. Uhr, L. W. M. M. Terstappen, *Clin. Cancer Res.* **2004**, *10*, 6897.
[100] D. Olmos, H. T. Arkenau, J. E. Ang, I. Ledaki, G. Attard, C. P. Carden, A. H. M. Reid, R. A'Hern, P. C. Fong, N. B. Oomen, et al., *Ann. Oncol.* **2009**, *20*, 27.
[101] P. A. J. Mendelaar, J. Kraan, M. Van, L. L. Zeune, L. W. M. M. Terstappen, E. Oomen-de Hoop, J. W. M. Martens, S. Sleijfer, *Mol. Oncol.* **2021**, *15*, 116.
[102] A. F. Sarioglu, N. Aceto, N. Kojic, M. C. Donaldson, M. Zeinali, B. Hamza, A. Engstrom, H. Zhu, T. K. Sundaresan, D. T. Miyamoto, et al., *Nat. Methods* **2015**, *12*, 685.
[103] M. Wendel, L. Bazhenova, R. Boshuizen, A. Kolatkar, M. Honnatti, E. H. Cho, D. Marrinucci, A. Sandhu, A. Perricone, P. Thistlethwaite, et al., *Phys. Biol.* **2012**, *9*, 016005.
[104] N. Aceto, *Biomed. J.* **2020**, *43*, 18.
[105] E. Schuster, R. Taftaf, C. Reduzzi, M. K. Albert, I. Romero-Calvo, H. Liu, *Trends Cancer* **2021**, *7*, 1020.
[106] M. Lim, S. Park, H. O. Jeong, S. H. Park, S. Kumar, A. Jang, S. Lee, D. U. Kim, Y. K. Cho, *Cancers* **2021**, *13*, 1.
[107] V. Yaghoubi Naei, E. Ivanova, W. Mullally, C. G. O'Leary, R. Ladwa, K. O'Byrne, M. E. Warkiani, A. Kulasinghe, *Clin. Transl. Immunol.* **2024**, *13*, e1516.
[108] P. Patil, Madhuprasad, T. Kumeria, D. Losic, M. Kurkuri, *RSC Adv.* **2015**, *5*, 89745.
[109] C. Li, W. He, N. Wang, Z. Xi, R. Deng, X. Liu, R. Kang, L. Xie, X. Liu, *Front. Bioeng. Biotechnol.* **2022**, *10*, 907232.
[110] P. Bankó, S. Y. Lee, V. Nagygyörgy, M. Zrínyi, C. H. Chae, D. H. Cho, A. Telekes, *J. Hematol. Oncol.* **2019**, *12*, 48.
[111] M. Stevens, A. Mentink, A. Nanou, F. A. W. Coumans, K. T. Isebia, J. Kraan, P. Hamberg, J. W. M. Martens, L. W. M. M. Terstappen, *Cytom. Part A* **2023**, *103*, 881.
[112] J. Kapeleris, A. Kulasinghe, M. E. Warkiani, C. Oleary, I. Vela, P. Leo, P. Sternes, K. O'Byrne, C. Punyadeera, *Transl. Lung Cancer Res.* **2020**, *9*, 1795.
[113] S. H. Au, J. Edd, D. A. Haber, S. Maheswaran, S. L. Stott, M. Toner, *Curr. Opin. Biomed. Eng.* **2017**, *3*, 13.
[114] M. Boya, T. Ozkaya-Ahmadov, B. E. Swain, C. H. Chu, N. Asmare, O. Civelekoglu, R. Liu, D. Lee, S. Tobia, S. Biliya, et al., *Nat. Commun.* **2022**, *13*, 1.
[115] Cancer Research UK, "*Blood Test, Full Blood Count*", https://www.cancerresearchuk.org/about-cancer/tests-and-scans/blood-tests, (accessed: March, 2025).
[116] J. C.-H. Hsieh, T. M.-H. Wu, *Tumor Metastasis*, InTech, London, United Kingdom **2016**, Ch. 8.
[117] V. Murlidhar, L. Rivera-Báez, S. Nagrath, *Small* **2016**, *12*, 4450.

[118] M. H. D. Neumann, H. Schneck, Y. Decker, S. Schömer, A. Franken, V. Endris, N. Pfarr, W. Weichert, D. Niederacher, T. Fehm, et al., *Biotechnol. Prog.* **2017**, *33*, 125.
[119] L. V. Sequist, S. Nagrath, M. Toner, D. A. Haber, T. J. Lynch, *J. Thorac. Oncol.* **2009**, *4*, 281.
[120] M. Trzpis, P. M. J. McLaughlin, L. M. F. H. De Leij, M. C. Harmsen, *Am. J. Pathol.* **2007**, *171*, 386.
[121] T.-Y. Na, L. Schecterson, A. M. Mendonsa, B. M. Gumbiner, *PNAS* **2020**, *117*, 5931.
[122] C. Mayo, F. G. Ortega, A. Giménez-Capitán, M. A. Molina-Vila, M. J. Serrano, S. Viteri, C. Costa, A. Gascó, J. Bertran-Alamillo, N. Karachaliou, et al., *Transl. Lung Cancer Res.* **2013**, *2*, 65.
[123] A. Satelli, S. Li, *Cell. Mol. Life Sci.* **2011**, *68*, 3033.
[124] A. C. W. Zannettino, K. M. Mrozik, O. W. Blaschuk, K. Vandyke, C. M. Cheong, *BMC Cancer* **2018**, *18*, 1.
[125] S. Loibl, L. Gianni, *Lancet* **2017**, *389*, 2415.
[126] S.-H. Belbina, M. R. Schmolze, S. Gereta, A. A. Laviana, *Front. Urol.* **2022**, *2*, 1.
[127] H. Li, Y. Xu, H. Li, *Oncotarget* **2017**, *8*, 62573.
[128] D. Lin, L. Shen, M. Luo, K. Zhang, J. Li, Q. Yang, F. Zhu, D. Zhou, S. Zheng, Y. Chen, et al., *Signal Transduct. Target Ther.* **2021**, *6*, 404.
[129] M. Lustberg, K. R. Jatana, M. Zborowski, J. J. Chalmers, *Recent Results Cancer Res.* **2012**, *195*, 97.
[130] C. J. Liao, C. H. Hsieh, H. M. Wang, W. P. Chou, T. K. Chiu, J. H. Chang, A. C. Chao, M. H. Wu, *RSC Adv.* **2017**, *7*, 29339.
[131] H. Kang, J. Kim, H. Cho, K. H. Han, *Micromachines* **2019**, *10*, 386.
[132] A. Mishra, T. D. Dubash, J. F. Edd, M. K. Jewett, S. G. Garre, N. Murat Karabacak, D. C. Rabe, B. R. Mutlu, J. R. Walsh, R. Kapur, et al., *Proc. Natl. Acad. Sci.* **2020**, *117*, 16839.
[133] L. Chen, A. M. Bode, Z. Dong, *Theranostics* **2017**, *7*, 2606.
[134] P. Y. Chu, C. H. Hsieh, M. H. Wu, *Front. Bioeng. Biotechnol.* **2020**, *8*, 1.
[135] P. Rostami, N. Kashaninejad, K. Moshksayan, M. S. Saidi, B. Firoozabadi, N. T. Nguyen, *J. Sci.: Adv. Mater. Devices* **2019**, *4*, 1.
[136] C. A. Lemaire, S. Z. Liu, C. L. Wilkerson, V. C. Ramani, N. A. Barzanian, K. W. Huang, J. Che, M. W. Chiu, M. Vuppalapaty, A. M. Dimmick, et al., *SLAS Technol.* **2018**, *23*, 16.
[137] M. E. Warkiani, B. L. Khoo, L. Wu, A. K. P. Tay, A. A. S. Bhagat, J. Han, C. T. Lim, *Nat. Protoc.* **2016**, *11*, 134.
[138] S. Gupta, A. Bit, n *Bioelectronics and Medical Devices: From Materials to Devices - Fabrication, Applications and Reliability*, Woodhead Publishing, Sawston, United Kingdom **2019**, Ch. 6.
[139] B. Çetin, D. Li, *Electrophoresis* **2011**, *32*, 2410.
[140] X. Ye, J. Zou, J. Chen, S. Luo, Q. Zhao, B. Situ, L. Zheng, Q. Wang, *Clin. Chim. Acta* **2023**, *547*, 117421.
[141] M. Pødenphant, N. Ashley, K. Koprowska, K. U. Mir, M. Zalkovskij, B. Bilenberg, W. Bodmer, A. Kristensen, R. Marie, *Lab Chip* **2015**, *15*, 4598.
[142] H. W. Hou, M. E. Warkiani, B. L. Khoo, Z. R. Li, R. A. Soo, D. S. W. Tan, W. T. Lim, J. Han, A. A. S. Bhagat, C. T. Lim, *Sci. Rep.* **2013**, *3*, 1259.
[143] H. Chen, *Sci. Rep.* **2018**, *8*, 4042.
[144] J. McGrath, M. Jimenez, H. Bridle, *Lab Chip* **2014**, *14*, 4139.
[145] K. Loutherback, J. D'Silva, L. Liu, A. Wu, R. H. Austin, J. C. Sturm, *AIP Adv.* **2012**, *2*, 042107.
[146] Z. Liu, F. Huang, J. Du, W. Shu, H. Feng, X. Xu, Y. Chen, *Biomicrofluidics* **2013**, *7*, 011801.
[147] Z. Liu, R. Chen, Y. Li, J. Liu, P. Wang, X. Xia, L. Qin, *Adv. Biosyst.* **2018**, *2*, 1800200.
[148] A. Hochstetter, R. Vernekar, R. H. Austin, H. Becker, J. P. Beech, D. A. Fedosov, G. Gompper, S. C. Kim, J. T. Smith, G. Stolovitzky, et al., *ACS Nano* **2020**, *14*, 10784.
[149] K. Loutherback, K. S. Chou, J. Newman, J. Puchalla, R. H. Austin, J. C. Sturm, *Microfluid. Nanofluid.* **2010**, *9*, 1143.
[150] T. Salafi, Y. Zhang, Y. Zhang, *Nanomicro Lett.* **2019**, *11*, 77.
[151] D. Holmes, G. Whyte, J. Bailey, N. Vergara-Irigaray, A. Ekpenyong, J. Guck, T. Duke, *Interface Focus* **2014**, *4*, 20140011.
[152] Z. Zhang, E. Henry, G. Gompper, D. A. Fedosov, *J. Chem. Phys.* **2015**, *143*, 243145.
[153] S. H. Au, J. Edd, A. E. Stoddard, K. H. K. Wong, F. Fachin, S. Maheswaran, D. A. Haber, S. L. Stott, R. Kapur, M. Toner, *Sci. Rep.* **2017**, *7*, 2433.
[154] Z. Liu, Y. Huang, W. Liang, J. Bai, H. Feng, Z. Fang, G. Tian, Y. Zhu, H. Zhang, Y. Wang, et al., *Lab Chip* **2021**, *21*, 2881.
[155] N. M. Karabacak, P. S. Spuhler, F. Fachin, E. J. Lim, V. Pai, E. Ozkumur, J. M. Martel, N. Kojic, K. Smith, P. I. Chen, et al., *Nat. Protoc.* **2014**, *9*, 694.
[156] J. P. Beech, K. Keim, B. D. Ho, C. Guiducci, J. O. Tegenfeldt, *Adv. Mater. Technol.* **2019**, *4*, 1900339.
[157] K. Torres-Castro, J. Jarmoshti, L. Xiao, A. Rane, A. Salahi, L. Jin, X. Li, F. Caselli, C. Honrado, N. S. Swami, *Adv. Mater. Technol.* **2023**, *2201463*, 2201463.
[158] N. Xiang, J. Wang, Q. Li, Y. Han, D. Huang, Z. Ni, *Anal Chem.* **2019**, *91*, 10328.
[159] R. Campos-González, A. M. Skelley, K. Gandhi, D. W. Inglis, J. C. Sturm, C. I. Civin, T. Ward, *SLAS Technol.* **2018**, *23*, 338.
[160] N. Tottori, T. Nisisako, *Sci. Rep.* **2023**, *13*, 4994.
[161] V. Calero, P. García-Sánchez, A. Ramos, H. Morgan, *J. Chromatogr. A* **2020**, *1623*, 461151.
[162] S. Khetani, M. Mohammadi, A. S. Nezhad, *Biotechnol. Bioeng.* **2018**, *115*, 2504.
[163] Y. T. Kang, I. Doh, Y. H. Cho, *Biomed. Microdevices* **2015**, *17*, 45.
[164] Y. Tang, J. Shi, S. Li, L. Wang, Y. E. Cayre, Y. Chen, *Sci. Rep.* **2014**, *4*, 1.
[165] Y. Kim, J. Bu, Y. H. Cho, I. T. Son, S. B. Kang, *J. Micromech. Microeng.* **2017**, *27*, 025015.
[166] Y. Liu, T. Xu, Y. Xu, D. Kang, L. Xu, J. Park, J. H. C. Chang, X. Zhang, A. Goldkorn, Y. C. Tai, *J. Micromech. Microeng.* **2015**, *25*, 104002.
[167] M. Hosokawa, H. Kenmotsu, Y. Koh, T. Yoshino, T. Yoshikawa, T. Naito, T. Takahashi, H. Murakami, Y. Nakamura, A. Tsuya, et al., *PLoS One* **2013**, *8*, e67466.
[168] S. Ribeiro-Samy, M. I. Oliveira, T. Pereira-Veiga, L. Muinelo-Romay, S. Carvalho, J. Gaspar, P. P. Freitas, R. López-López, C. Costa, L. Diéguez, *Sci. Rep.* **2019**, *9*, 1.
[169] S. Zhang, Y. Wang, C. Yang, J. Zhu, X. Ye, W. Wang, *Nanotechnol. Precis. Eng.* **2022**, *5*, 013003.
[170] N. Kamyabi, J. Huang, J. J. Lee, V. Bernard, A. Semaan, B. Stephens, M. W. Hurd, S. A. Vanapalli, A. Maitra, P. A. Guerrero, *Biomicrofluidics* **2019**, *13*, 044111.
[171] J. Zhang, K. Chen, Z. H. Fan, *Adv Clin Chem*, Clinical Laboratory Partners, Newington, CT **2016**, Ch. 1.
[172] C. Dolfus, N. Piton, E. Toure, J. C. Sabourin, *Chin. J. Cancer Res.* **2015**, *27*, 479.
[173] A. Xiang, M. Xue, F. Ren, L. Wang, Z. Ye, D. Li, Q. Ji, G. Ji, Z. Lu, *Oncol. Rep.* **2020**, *43*, 1975.
[174] D. L. Adams, P. Zhu, O. V. Makarova, S. S. Martin, M. Charpentier, S. Chumsri, S. Li, P. Amstutz, C. M. Tang, *RSC Adv.* **2014**, *4*, 4334.
[175] M. Wu, A. Ozcelik, J. Rufo, Z. Wang, R. Fang, T. Jun Huang, *Microsyst. Nanoeng.* **2019**, *5*, 32.
[176] X. Ding, P. Li, S. C. S. Lin, Z. S. Stratton, N. Nama, F. Guo, D. Slotcavage, X. Mao, J. Shi, F. Costanzo, et al., *Lab Chip* **2013**, *13*, 3626.
[177] F. Olm, A. Urbansky, J. H. Dykes, T. Laurell, S. Scheding, *Sci. Rep.* **2019**, 1.

[178] X. Lu, A. Martin, F. Soto, P. Angsantikul, J. Li, C. Chen, Y. Liang, J. Hu, L. Zhang, J. Wang, *Adv. Mater. Technol.* **2019**, *4*, 1800374.
[179] P. Li, Z. Mao, Z. Peng, L. Zhou, Y. Chen, P. Huang, C. I. Truica, J. J. Drabick, W. S. El-Deiry, M. Dao, et al., *Proc. Natl. Acad. Sci. U. S. A.* **2015**, *112*, 4970.
[180] E. Undvall Anand, C. Magnusson, A. Lenshof, Y. Ceder, H. Lilja, T. Laurell, *Anal. Chem.* **2021**, *93*, 17076.
[181] J. F. Chen, H. Ho, J. Lichterman, Y. T. Lu, Y. Zhang, M. A. Garcia, S. F. Chen, A. J. Liang, E. Hodara, H. E. Zhau, et al., *Cancer* **2015**, *121*, 3240.
[182] C. Magnusson, P. Augustsson, E. Undvall Anand, A. Lenshof, A. Josefsson, K. Welén, A. Bjartell, Y. Ceder, H. Lilja, T. Laurell, *Anal. Chem.* **2024**, *96*, 6914.
[183] E. A. Kwizera, M. Sun, A. M. White, J. Li, X. He, *ACS Biomater. Sci. Eng.* **2021**, *7*, 2043.
[184] F. S. Iliescu, W. J. Sim, H. Heidari, D. P. Poenar, J. Miao, H. K. Taylor, C. Iliescu, *Electrophoresis* **2019**, *40*, 1457.
[185] S. Shim, K. Stemke-Hale, J. Noshari, F. F. Becker, P. R. C. Gascoyne, *Biomicrofluidics* **2013**, *7*, 011808.
[186] P. R. C. Gascoyne, S. Shim, J. Noshari, F. F. Becker, K. Stemke-Hale, *Electrophoresis* **2013**, *34*, 1042.
[187] S. H. Kim, H. Ito, M. Kozuka, M. Hirai, T. Fujii, *Biomicrofluidics* **2017**, *11*, 054114.
[188] S. Shim, K. Stemke-Hale, A. M. Tsimberidou, J. Noshari, T. E. Anderson, P. R. C. Gascoyne, *Biomicrofluidics* **2013**, *7*, 011807.
[189] G. R. Pesch, M. Lorenz, S. Sachdev, S. Salameh, F. Du, M. Baune, P. E. Boukany, J. Thöming, *Sci. Rep.* **2018**, *8*, 1.
[190] S. Bhattacharya, T. C. Chao, N. Ariyasinghe, Y. Ruiz, D. Lake, R. Ros, A. Ros, *Anal. Bioanal. Chem.* **2014**, *406*, 1855.
[191] G. R. Pesch, F. Du, *Electrophoresis* **2021**, *42*, 134.
[192] P. R. C. Gascoyne, S. Shim, *Cancers* **2014**, *6*, 545.
[193] V. Gupta, I. Jafferji, M. Garza, V. O. Melnikova, D. K. Hasegawa, R. Pethig, D. W. Davis, *Biomicrofluidics* **2012**, *6*, 024133.
[194] P. R. C. Gascoyne, J. Noshari, T. J. Anderson, F. F. Becker, *Electrophoresis* **2009**, *30*, 1388.
[195] Y. Huang, J. Yang, X.-B. Wang, F. F. Becker, P. R. C. Gascoyne, *J. Hematother. Stem Cell Res.* **1999**, *5*, 481.
[196] P. Balasubramanian, R. J. Kinders, S. Kummar, V. Gupta, D. Hasegawa, A. Menachery, S. M. Lawrence, L. Wang, K. Ferry-Galow, D. Davis, et al., *PLoS One* **2017**, *12*, e0175414..
[197] D. J. O'Shannessy, D. W. Davis, K. Anderes, E. B. Somers, *Biomark Insights* **2016**, *11*, 7.
[198] F. Le Du, T. Fujii, K. Kida, D. W. Davis, M. Park, D. D. Liu, W. Wu, M. Chavez-MacGregor, C. H. Barcenas, V. Valero, et al., *PLoS One* **2020**, *15*, e0229903.
[199] E. A. Henslee, M. B. Sano, A. D. Rojas, E. M. Schmelz, R. V. Davalos, *Electrophoresis* **2011**, *32*, 2523.
[200] T. A. Douglas, J. Cemazar, N. Balani, D. C. Sweeney, E. M. Schmelz, R. V. Davalos, *Electrophoresis* **2017**, *38*, 1507.
[201] M. Li, R. K. Anand, *J. Am. Chem. Soc.* **2017**, *139*, 8950.
[202] I. F. Cheng, W. L. Huang, T. Y. Chen, C. W. Liu, Y. De Lin, W. C. Su, *Lab Chip* **2015**, *15*, 2950.
[203] J. An, J. Lee, S. H. Lee, J. Park, B. Kim, *Anal. Bioanal. Chem.* **2009**, *394*, 801.
[204] E. A. Kwizera, W. Ou, S. Lee, S. Stewart, J. G. Shamul, J. Xu, N. Tait, K. H. R. Tkaczuk, X. He, *ACS Nano* **2022**, *16*, 11374.
[205] G. I. Russo, N. Musso, A. Romano, G. Caruso, S. Petralia, L. Lanzanò, G. Broggi, M. Camarda, *Cancers* **2022**, *14*, 198.
[206] S. Ju, C. Chen, J. Zhang, L. Xu, X. Zhang, Z. Li, Y. Chen, J. Zhou, F. Ji, L. Wang, *Biomark. Res.* **2022**, *10*, 58.
[207] M. Antfolk, T. Laurell, *Anal. Chim. Acta* **2017**, *965*, 9.
[208] P. G. Bonacci, G. Caruso, G. Scandura, C. Pandino, A. Romano, G. I. Russo, R. Pethig, M. Camarda, N. Musso, *Transl. Oncol.* **2023**, *28*, 101599.
[209] A. Menachery, R. Pethig, *IEE Proc. Nanobiotechnol.* **2005**, *152*, 145.
[210] A. Mehran, P. Rostami, M. S. Saidi, B. Firoozabadi, N. Kashaninejad, *Biosensors* **2021**, *11*, 406.
[211] J. Jiang, H. Zhao, W. Shu, J. Tian, Y. Huang, Y. Song, R. Wang, E. Li, D. Slamon, D. Hou, et al., *Sci. Rep.* **2017**, *7*, 1.
[212] J. Wang, Y. Li, R. Wang, C. Han, S. Xu, T. You, Y. Li, J. Xia, X. Xu, D. Wang, et al., *ACS Appl. Mater. Interfaces* **2021**, *13*, 30174.
[213] T. Akashi, T. Okumura, K. Terabayashi, Y. Yoshino, H. Tanaka, T. Yamazaki, Y. Numata, T. Fukuda, T. Manabe, H. Baba, et al., *Oncol. Lett.* **2023**, *26*, 320.
[214] M. Pelle, A. A. K. Das, L. A. Madden, V. N. Paunov, *Adv. Biosyst.* **2020**, *4*, 1.
[215] B. H. Wunsch, K. Y. Hsieh, S. C. Kim, M. Pereira, S. Lukashov, C. Scerbo, J. M. Papalia, E. A. Duch, G. Stolovitzky, S. M. Gifford, et al., *Adv. Mater. Technol.* **2021**, *6*, 1.
[216] J. Chung, H. Shao, T. Reiner, D. Issadore, R. Weissleder, H. Lee, *Adv. Healthc. Mater.* **2012**, *1*, 432.
[217] Y. Liu, T. Li, M. Xu, W. Zhang, Y. Xiong, L. Nie, Q. Wang, H. Li, W. Wang, *Lab Chip* **2019**, *19*, 68.
[218] J. Shim, J. Bu, M. Lee, Y. Cho, T. Kim, J. Bu, *Sens. Actuators, B* **2020**, *321*, 128369.
[219] T. Huang, C. P. Jia, Jun Yang, W. J. Sun, W. T. Wang, H. L. Zhang, H. Cong, F. X. Jing, H. J. Mao, Q. H. Jin, et al., *Biosens. Bioelectron.* **2014**, *51*, 213.
[220] Y. Quan, Z. Zhu, D. Tang, S. Zhu, C. Wang, K. Chen, Z. Ni, *Sep. Purif. Technol.* **2022**, *296*, 121349.
[221] X. Fan, C. Jia, J. Yang, G. Li, H. Mao, Q. Jin, *Biosens. Bioelectron.* **2015**, *71*, 380.
[222] P. Li, Z. Mao, Z. Peng, L. Zhou, Y. Chen, P. Huang, C. I. Truica, **2015**, *112*, 4970.
[223] I. González, J. Earl, L. J. Fernández, B. Sainz, A. Pinto, R. Monge, S. Alcalá, A. Castillejo, J. L. Soto, A. Carrato, *Micromachines* **2018**, *9*, 129.
[224] S. Karthick, P. N. Pradeep, P. Kanchana, A. K. Sen, *Lab Chip* **2018**, *18*, 3802.
[225] P. Augustsson, C. Magnusson, M. Nordin, H. Lilja, T. Laurell, *Anal. Chem.* **2012**, *84*, 7954.
[226] S. Bin Huang, M. H. Wu, Y. H. Lin, C. H. Hsieh, C. L. Yang, H. C. Lin, C. P. Tseng, G. Bin Lee, *Lab Chip* **2013**, *13*, 1371.

Gürhan Özkayar is a postdoctoral researcher at Soft Matter Group in the Department of Chemical Engineering at Delft University of Technology. He received his B.Sc. and M.Sc. degrees in Biomedical Engineering from Baskent University, Turkey, in 2009 and from Middle East Technical University (METU), Turkey, in 2015, respectively. He worked as an R&D Engineer at Mikro Biyosistemler Inc. (2015–2019) developing microfluidic devices for particle separation. His Ph.D. studies focused on integration and miniaturization of microfluidic systems in the Department of Precision and Microsystems Engineering at Delft University of Technology (2019–2023). His current research focuses on label-free isolation of heterogeneous CTCs.

Esma Derin is currently pursuing her Ph.D. in the Bioanalytics Group at the Department of Biosystems Science and Engineering, ETH Zurich, where she is working on microfluidics and artificial cells. She also gained experience in CTC isolation using microfluidics at TU Delft. She received her Master's degree in Materials Science and Nanotechnology from Bilkent University in 2022. Her thesis focused on extracellular vesicle isolation and detection using metamaterial-based plasmonic biosensors with signal enhancement strategies, and it was supervised by Asst. Prof. Fatih Inci.

Georg R. Pesch is an Assistant Professor in Chemical and Bioprocess Engineering at University College Dublin (UCD). He received his PhD in Production Engineering in 2018 from the University of Bremen. From 2019 to 2020, he was a post-doctoral fellow in the Chemical Engineering Department of Delft University of Technology, working on label-free cancer isolation methods using microfluidic dielectrophoresis. From 2018 to 2022, he was a group leader in the Chemical Process Engineering section of the University of Bremen. He joined UCD in 2022, where he is working on high-throughput electrokinetic methods for particle separation.

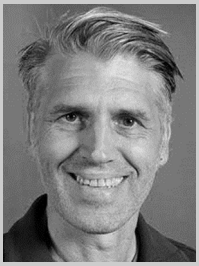

John W. M. Martens studied (1982–1988) and received his PhD (1994) at Wageningen University, the Netherlands. After being a postdoc in Molecular Endocrinology at Erasmus MC and USCF (1994–2001), he specialized on translational cancer genomics research (full professor since 2017) in the Dept. of Medical Oncology at the Erasmus MC, Rotterdam, the Netherlands. His ambition is 1) to discover new prognostic and predictive markers for breast and colorectal cancer and 2) to gain insight into the different molecular mechanisms underlying disease heterogeneous and associated development treatment resistance, ultimately to offer patients the best choice of treatment possible.

Peter ten Dijke received his Ph.D. degree in 1991 from Wageningen University, the Netherlands, based on his research on the identification of TGF-β3 performed at Oncogene Science, Inc., New York, USA. He did his postgraduate studies with Kohei Miyazono and Carl-Henrik Heldin at the Ludwig Institute for Cancer Research (LICR), Uppsala, Sweden. In 1999, he moved to the Netherlands Cancer Institute, Amsterdam, and thereafter in 2005 became a professor at Leiden University Medical Center, Leiden, the Netherlands, and in 2018 an Oncode Institute investigator. His laboratory studies how subverted TGF-β family signaling is involved in cancer cell plasticity.

Pouyan E. Boukany is an associate professor in the Chemical Engineering Department at Delft University of Technology (TU Delft). He obtained his Ph.D. in Polymer Science from the University of Akron in 2008. Subsequently, he was awarded a postdoctoral fellowship to join the Center for Affordable Nanoengineering of Polymeric Biomedical Devices at Ohio State University. In 2011, he became a principal investigator at TU Delft, where he pioneered a new research direction at the intersction of microfluidics, soft matter, and biology. His work focuses on understanding the dynamics and transport of biological systems and biomolecules at the micro/nanoscale.